CHARACTERIZATION AND STUDY OF THE VISCOUS BEHAVIOR OF CuO-H_2O, EG (ETHYLENE GLYCOL) BASED NANOFLUID

Thesis submitted in the partial fulfillment of requirement for the award of degree of

Master of Engineering

in

THERMAL ENGINEERING

Submitted by:

VISHAL BHALLA

Roll No: 801083027

Under the guidance of

Mr. Kundan Lal
Assistant Professor, MED
TU, Patiala-147004

MECHANICAL ENGINNERING DEPARTMENT
THAPAR UNIVERSITY
PATIALA – 147004

2012

DECLARATION

I hereby declare that thesis entitled **"Characterization and Study of the Viscous Behaviour of CuO-H_2O, EG (Ethylene Glycol) Based Nanofluid"** is an authentic record of my study carried out as requirements for the award of degree of **M.Tech. (Thermal Engineering)** at **Thapar University, Patiala**, under the guidance of **Mr. Kundanlal**, Assistant Professor, **Department of Mechanical Engineering**, Thapar University, Patiala during **August 2011 to July 2012**. The matter embodied in this thesis has not been submitted in part or full to any other university or institute for the award of any degree.

Vishal Bhalla

(VISHAL BHALLA)

This is to certify that above declaration made by the student concerned is correct to the best of my knowledge and belief.

5/7/12

(MR. KUNDAN LAL)

Assistant Professor, MED
TU, Patiala-147004

Countersigned by:

(DR. AJAY BATISH)
Head of Department
Department of Mechanical Engineering
Thapar University
Patiala-147004

(DR. S.K. MOHAPATRA)
Dean of Academic Affairs
Thapar University
Patiala-147004

ACKNOWLEDGEMENTS

Words are often less to revels one.s deep regards. With an understanding that work like this can never be the outcome of a single person, I take this opportunity to express my profound sense of gratitude and respect to all those who helped me through the duration of this work.

This work would not have been possible without the encouragement and able guidance of supervisor Mr. Kundan Lal. Their enthusiasm and optimism made this experience both rewarding and enjoyable. Most of the novel ideas and solutions in this work are the result of our numerous stimulating discussions. Their feedback and editorial comments were also invaluable for the writing of this thesis.

With deep sense of gratitude I express my sincere thanks to Mr. Bhupinderpal , Research scholar in Department of Chemistry, without which this work would not have been reality.

I take pride of myself being son of ideal parents for their everlasting desire, sacrifice, affectionate blessings, and help, without which it would not have been possible for me to complete my studies.

I am also very grateful to my all friends and colleague (Pooja Singh, Priyanka Gupta, Chitrarth Kishore) for accompanying me during the most outstanding year of my life and standing by me in everysituation.

I would like to thank to all the faculty members and employees of Mechanical Engineering Department, Thapar Univeristy, Patiala for their everlasting support.

Last but not least, I would like to thank God for all good deeds.

Vishal Bhalla

(Vishal Bhalla)

ABSTRACT

Nanofluids are suspensions of nanoparticles in base fluids, a new challenge for thermal sciences provided by nanotechnology. CuO nanocrystals with different shapes, i.e. irregular nanoparticles, nanoplatelets, have been synthesized by controlling a few critical synthesis parameters to explore their catalytic properties. The tested fluids are prepared by dispersing the CuO into water and ethylene glycol at four different concentrations 0.005 %, 0.05%, 0.01% and 0.1% and the mixture of ethylene glycol and water at two different concentrations 0.005% and 0.05%. Viscosity of nanofluid is measured by Brookfield Viscometer (LV DV-IIICP). Experimental results show that viscosity of nanofluids is higher than the base fluid and with increase in concentration it increases and also it is observed that viscosity of nanofluid decreases with increase in temperature. The result shows that the there is a rapid settling of CuO nanoparticles in water as compared to ethylene glycol. Ethylene glycol shows Newtonian behavior even at 50^{o}C and also with increase in temperature. The mixture of ethylene glycol and water shows the 7.25% increase in its viscosity when CuO nanoparticles are added at 25^{o}C. The shear thinning behaviour of nanofluid is observed with increase in temperature (25^{o}C to 50^{o}C) and volumetric concentration (0.001% to 0.1%) takes place when the temperature increases even with increase in volumetric concentration.

INDEX

CONTENTS Page No.

Contents i-iv

List of figures v-viii

List of tables ix

Abbreviations x

CHAPTER 1: INTRODUCTION

1.1 Introduction 1

1.2 Nanofluids 1

1.3 Importance of Nanosize 2

1.4 Manufacturing of Nanofluid 3

1.5 Materials for Nanoparticles and Nanofluids 3

1.6 Surfactants 4

CHAPTER 2: LITERATURE REVIEW

2.1 Introduction 6

2.2 Thermophysical Properties of Nanofluids 6

2.3 Nanofluids Preparation and Characterization 7

2.3.1 Preparation 7

2.3.2 Characterization 8

2.4 Factors Effecting Viscosity of Nanofluids 9

2.5 Viscosity Models for Nanofluids 18

2.5 Objective 22

CHAPTER 3: SYNTHESIS AND CHARACTERIZATION

3.1 Synthesis 23

3.2 Experimental Details 23

3.3 Results and Discussion 24

3.4 Characterization 25

3.5 Different Methods of Characterization 25

3.6 Types of Characterization Methods 29

3.6.1 Optical probe characterization techniques 30

3.6.2 Electron probe characterization methods 30

3.6.3 Scanning probe characterization techniques 31

3.6.4 Spectroscopic characterization methods 31

3.6.5 Ion –particle characterization techniques 32

3.6.6 Thermodynamic characterization methods 32

CHAPTER 4: INSTRUMENTS USED FOR EXPERIMENTAL WORK

4.1 Ultrasonic Processor/ Sonicator 34

4.2 X-ray Powder Diffraction 35

4.2.1 Fundamental principles of x-ray powder diffraction 35

4.3 Scanning Electron Microscope 36

4.3.1 Working of scanning electron microscope 37

4.3.2 Preparation of sample 38

4.4 Transmission Electron Microscopy 38

4.4.1 Usage of transmission electron microscopy 38

4.4.2 Principal of operation 40

4.5 Viscometer 41

CHAPTER 5: METHODOLGY

5.1 Introduction 42

5.2 Materials Used for Preparing Nanofluids 42

5.3 Preparation of Nanofluids 42
5.4 Measurement of Viscosity 43
CHAPTER 6: RESULTS AND DISCUSSION
6.1 Viscous Behavior of Water 45
6.2 Viscous Behavior of Ethylene Glycol 47
6.3 Viscous Behaviour of Ethylene Glycol (EG) with CuO Nanoparticles 48
6.3.1 Ethylene glycol + CuO with 0.005% volumetric concentration 48
6.3.2 Ethylene glycol + CuO with 0.01% volumetric concentration 49
6.3.3 Ethylene glycol + CuO with 0.05% volumetric concentration 50
6.3.4 Ethylene glycol + CuO with 0.1% volumetric concentration 51
6.4 Ethylene glycol (60): Water (40) 53
6.4.1 Ethylene glycol (60): water (40) with CuO in 0.005% volumetric concentration 54
6.4.2 Ethylene glycol (60): water (40) with CuO in 0.05% volumetric concentration 55
CHAPTER 7 : CONCLUSION 58
CHAPTER 8 : APPLICATION AND FUTURE SCOPE
8.1 Introduction 59
8.2 Future Scope 60
REFERENCES 61
ANNEXTURE-I 68
ANNEXTURE-II 75

List of figures

FIGURE NO.	ITEM DESCRIPTION	PAGE NO.
2.1	Effective viscosity v/s temperature (K) at different volumetric concentrations	9
2.2	Viscosity v/s partial volume fraction for CuO and Al_2O_3 with different diameters	10
2.3	Effective viscosity v/s temperature for different volumetric concentration	11
2.4	Effective viscosity v/s temperature for different volumetric concentrations	11
2.5	Viscosity of the silicon dioxide nanofluid (50 nm) with 6% volume concentration against shear rate for varying temperatures from -35 to 50 ^{0}C	12
2.6	Experimental values of viscosity for varying volume concentrations of silicon dioxide nanofluids (50 nm) with respect to temperature	12
2.7	DVI against temperature for varying concentrations of silicon dioxide nanofluids (50 nm)	13
2.8	Effect of silicon dioxide nanoparticle diameter on nano-fluid viscosity for varying temperature	14
2.9	Viscosity ratio v/s volumetric concentration	21
3.1	XRD results	24
3.2	SEM Image	24
3.3	SEM Image	24
4.1	Ultra sonicator	34
4.2	X-Ray Diffraction	36
4.3	Scanning Electron Microscopy	37
4.4	X-Ray ejection from the sample	37

4.5	The schematic outline of a TEM	39
4.6	Electron source of a TEM	39
5.1	XRD result for CuO nanoparticle diameter 40 nm	42
5.2	CuO sample with different volumetric concentrations	43
5.3	Arrangement of water bath and viscometer	44
6.1	Shear stress v/s shear rate at different temperatures	45
6.2	Viscosity v/s shear rate at different temperatures	46
6.3	Shear stress v/s shear rate at different temperatures	47
6.4	Viscosity v/s shear rate at different temperatures	47
6.5	Shear stress v/s shear rate for same volumetric concentration (0.005%) at different temperatures	48
6.6	Viscosity v/s shear rate for same volumetric concentration (0.005%) at different temperatures	49
6.7	Shear stress v/s shear rate for same volumetric concentration (0.01%) at different temperatures	49
6.8	Viscosity v/s shear rate for same volumetric concentration (0.01%) at different temperatures	50
6.9	Shear stress v/s shear rate for same volumetric concentration (0.05%) at different temperatures	50
6.10	Viscosity v/s shear rate for same volumetric concentration (0.05%) at different temperatures	51
6.11	Shear stress v/s shear rate for same volumetric concentration (0.1%) at different temperatures	51
6.12	Viscosity v/s shear rate for same volumetric concentration (0.1%) at different temperatures	52

6.13	Shear stress v/s shear rate at different temperatures	53
6.14	Viscosity v/s shear rate at different temperatures	53
6.15	Shear stress v/s shear rate for same volumetric concentration (0.005%) at different temperatures	54
6.16	Viscosity v/s shear rate for same volumetric concentration (0.005%) at different temperatures	54
6.17	Shear stress v/s shear rate for same volumetric concentration (0.05%) at different temperatures	55
6.18	Viscosity v/s shear rate for same volumetric concentration (0.05%) at different temperatures	55
6.19	Viscosity v/s temperature for CuO mixed with water at various concentrations	56
6.20	Viscosity v/s temperature for CuO mixed with ethylene glycol at various concentrations	57
6.21	Viscosity v/s temperature for water mixed with ethylene glycol at various concentrations	57
6.22	Viscosity v/s volumetric concentration at different temperatures	58

LIST OF TABLES

Table no.	Item Description	Page no.
1.1	Comparison of Microparticles and Nanoparticles	2
2.1	Summary of the effective viscosity data reported by various research groups	15
2.2	Summary of commonly used models	18
3.1	Optical (Imaging) Probe Characterization Methods	25
3.2	Electron Probe Characterization Methods	25
3.3	Scanning Probe Characterization Methods	26
3.4	Photon (Spectroscopic) Probe Characterization Methods	27
3.5	Ion- particle Probe Characterization Methods	28
3.6	Thermodynamic Characterization Methods	29

ABBREVATION

Al_2O_3	Aluminum Oxide
CuO	Copper Oxide
EG	Ethylene Glycol
Fe_2O_3	Ferrous Oxide
H_2O	Water
MWCNT	Multi-walled carbon nanotube
PCS	Photon correlation spectroscopy
PLC	Programmable Logic Controller
SANS	Small angle neutron scattering
SAXS	Small angle x-ray scattering
SEM	Scanning Electron Microscopy
SPM	Scanning probe microscopy
TEM	Transmission Electron Microscopy
TiO_2	Titanium Oxide
XRD	X-Ray Diffrection
XPCS	X-ray photon correlation spectroscopy
μ_{eff}	Effective viscosity
∅	Volumetric concentration

CHAPTER 1

INTRODUCTION

1.1Introduction

Nanofluids are colloidal solution of solid nanoparticles in which dimensions of nanomaterials are in nano range (1-100 nm). It has been observed that nanofluids exhibit superior thermal properties as compared to the conventional fluids [1-3]. One reason for this is that nanoparticles have larger surface area and smaller size, possess a potential to further improve heat-transfer capabilities. It has been found that they have lower viscosity than the micron-sized particle-liquid suspensions, thus reducing pressure drop in the flow channel and saving the pumping power.

The experiments on the nanofluid viscosity [4-5] demonstrated up to 90% increment in a 5% volume fraction nanofluid compared with the base liquid. Like other factors, Viscosity is also one of the property which influences the heat transfer properties of the nanofluids. Nanofluids are preferred as cooling fluids because of their improved heat transfer capabilities. Since most of the cooling methods used, involve forced circulation of the coolant and increase in the properties of the fluids, specially viscosity will result in increased pumping power. The experimental investigations made so far show that the viscosity increases for nanofluid is higher than the predicted from Einstein, Brinkman, and Batchelor models [6-11].

1.2 Nanofluids

Nanofluids (Nanoparticle fluid suspensions) is the term coined by Choi (1995) to describe this new class of nanotechnology based heat transfer fluids that exhibit thermal properties superior to those of their host fluids or conventional particle fluid suspension [12].Nanofluids are engineered by suspending nanoparticles with the average size below 100 nm in traditional heat transfer fluids such as water, oil and ethylene glycol. When a small amount of nanoparticles, are added in the host fluids, can provide a dramatic change in the properties of host fluids. Nanofluid technology is a new interdisplinary field of great importance, where nanotechonogy, nanoscience and thermal engineering meet. The aim of the nanofluids is to achieve the highest possible thermal properties at smallest possible concentrations by uniform dispersion and stable suspension of nanoparticles in the host fluids. These nanoparticles can possess properties that are

substantially different from their parent materials like CuO possesses different properties from Cu.

Three methods of generating these nanofluids are available: creating them from chemical precipitation, purchasing the nanoparticles in powder form and mix them with the base fluid, and direct purchase of prepared nanofluids.

1.3 Importance of Nanosize

The major problem with the use of large particles is the rapid settling of these particles in fluids. Other problems are abrasion and clogging to the channels through which they are made to flow. These problems are highly undesirable for many practical cooling applications. The nanofluids are leaders in overcoming these problems because nanoparticles get stabled at nanoscale rather than the millimeter or micrometer sized particles. Compared with microparticles the nanoparticles suspended for a longer time and possess a much higher surface area. The surface/volume ratio of nanoparticles is 1000 times larger than that of microparticles. The high surface area of nanoparticles enhances the heat conduction of nanofluids since heat transfer occurs on the surface of the particle. Other benefits of using nanoparticles include decreased pumping power, reduced inventory of heat transfer fluids and significant energy savings.

In the nanofluids the size is the most important factor because it is used to increase the thermal properties as well as the suspension stability of the nanoparticles. The nanotechnology offers excellent prospects for producing a new type of heat transfer fluid that has an excellent thermal properties and cooling capacity. Table 1.1 contrasts suspension of microparticles and nanoparticles and shows the benefits of nanofluids containing nanoparticles. Other factors which influence the thermo physical properties of nanofluids are: shape, material, base fluid, surfactants, temperature, volumetric concentration, dispersants, pH value etc.

Table 1.1 Comparison of Microparticles and Nanoparticles [12]

	Microparticles	Nanoparticles
Stability	Settle	Stable (remain in suspension almost indefinitely)
Surface/volume ratio	1	1000 times larger than that of

		microparticles
Conductivity[a]	Low	High
Clog to microchannel	Yes	No
Erosion	Yes	No
Pumping Power	Large	Small
Nanoscale Phenomena	No	Yes

[a] At the same volume fraction.

The above table shows that conductivity, stability and surface/volume ratio of nanoparticles is more than the microparticles and there is least problem of clogging and erosion in nanoparticles.

1.4 Manufacturing of Nanofluids

There are commonly two methods which are used to fabricate nanoparticles 1. Physical process 2. Chemical process. The physical process includes inert gas condensation [87] and mechanical grinding. Chemical processes include chemical vapour deposition, chemical precipitation, micro emulsions, thermal spray and spray prolysis. Stable and highly conductive nanofluids are produced by one and two step production methods.

The two step method first makes nanoparticles by using either physical or chemical process and then disperse them in the base fluid. The one step method simultaneously makes and disperse nanoparticles directly into the base fluid. In two step method, to create a stable suspension is one of the key issue, as in this method the particles, they have tendency to agglomerate.

1.5 Materials for Nanoparticles and Fluids

Nanostructured or nanophase materials are made of nanometer sized substances engineered on the atomic or molecular scale to produce either new or enhanced physical properties, which are not exhibited by conventional bulk solids. So the particles smaller than 100 nm exhibit different properties as compared with the conventional solids. The thermal, mechanical, optical, magnetic and electrical properties of nanophase materials are more superior than those materials have coarse grain structure.

Nanoparticle material types: Nanoparticles used in nanofluiuds have been made of various materials, such as oxide ceramics (Al_2O_3, CuO), TiO_2, nitride ceramics(AlN,SiN), carbide

ceramics (SiC,TiC), metals (Cu,Ag,Au), semiconductors (TiO_2,SiC), Cabon nanotubes and composite materials such as alloyed nanoparticles $Al_{60}Cu_{30}$.

Host liquid types. Many types of liquids, such as water, ethylene glycol and oil have been used as host liquids in nanofluids.

1.6 Surfactants

Surfactants are usually organic compounds that are amphiphilic, means they contain both hydrophobic groups (their *tails*) and hydrophilic groups (their *heads*). Therefore, a surfactant molecule contains both a water insoluble (or oil soluble) component and a water soluble component. Surfactant molecules will diffuse in water and adsorb at interfaces between air and water or at the interface between oil and water, in the case where water is mixed with oil. The insoluble hydrophobic group may extend out of the bulk water phase, into the air or into the oil phase, while the water soluble head group remains in the water phase. This alignment of surfactant molecules at the surface modifies the surface properties of water at the water/air or water/oil interface.

Classification of Surfactants

From the commercial point of view surfactants are often classified according to their use.
However, this is not very useful because many surfactants have several uses, and confusions may arise from that. The most accepted and scientifically sound classification of surfactants is based on their dissociation in water.

Anionic surfactants : Anionic surfactants are dissociated in water in an amphiphilic anion, and a cation which is in general an alkaline metal (Na+, K+) or a quaternary ammonium. They are the most commonly used surfactants. They include alkylbenzene sulfonates (detergents), (fatty acid) soaps, lauryl sulfate (foaming agent), di-alkyl sulfosuccinate (wetting agent), lignosulfonates (dispersants) etc.

Nonionic surfactants: Nonionic surfactants do not ionize in aqueous solution, because their hydrophilic group is of a nondissociable type, such as alcohol, phenol, ether, ester, or amide. A large proportion of these nonionic surfactants are made hydrophilic by the presence of a

polyethylene glycol chain, obtained by the polycondensation of ethylene oxide. They are called polyethoxylated nonionics.

Cationic surfactants: Cationic surfactants are dissociated in water into an amphiphilic cation and an anion, most often of the halogen type. A very large proportion of this class corresponds to nitrogen compounds such as fatty amine salts and quaternary ammoniums, with one or several long chain of the alkyl type, often coming from natural fatty acids.

When a single surfactant molecule exhibit both anionic and cationic dissociations it is called **amphoteric** or **zwitterionic**. This is the case of synthetic products like betaines or sulfobetaines and natural substances such as aminoacids and phospholipids. Some amphoteric surfactants are insensitive to pH, whereas others are cationic at low pH and anionic at high pH, with an amphoteric behavior at intermediate pH.

Commonly used surfactants :

Sodium Dodecyl BenzeneSulfonate, Dimethyl Ether of Tetradecyl Phosphonic, Lauryl Mono-Ethanol, Glycerol Diester (diglyceride), Dodecyl Betaine, Abietic Acid, Polyethoxylated Octyl Phenol, Sorbitan Monoester, N-Dodecyl Piridinium Chloride.

Surfactants role in nanofluids

They are added to get stable suspension. The addition of surfactant has different-2 effects. The surfactant properties depend on the base fluid’s pH value. Their addition change the pH value of nanofluid and because of that magnitude of same charge on the particle increases which cause repulsion among the suspended nanoparticles and hence increase the stability of solution.

CHAPTER 2

LITERATURE SURVEY

2.1 Introduction

Nanofluid research could lead to a major breakthrough in developing next-generation coolants for a number of engineering applications. Better ability to manage the thermal properties translates into greater energy efficiency, smaller and lighter thermal systems and lower operating costs. Various studies on nanofluids were carried out by many researchers in the past.

This chapter reviews the previous published literatures, which lays foundation and basis for further work in this investigation. This helps to give a better understanding about the topic and also acts as a guideline for this thesis. The major focus of the following study is on the nanofluids and to check the viscous behavior with various fluids. This section deals with literature review on nanofluids, its preparation and characterization, thermo-physical properties of nanofluids.

2.2 Thermophysical Properties of Nanofluids

Nanofluids were found to exhibit higher thermo-physical properties such as thermal conductivity, thermal diffusivity and viscosity than those of base fluids. Heat transfer enhancement in a solid-fluid two-phase flow has been investigated for many years. Research on gas particle flow[23-26] showed that by adding particles, especially small particles in gas, the convection heat transfer coefficient can be greatly increased. The enhancement of heat transfer, in addition to the possible increase in the effective thermal conductivity, was mainly due to the reduced thickness of the thermal boundary layer. In the processes involving liquid-vapor phase change, particles may also reduce the thickness of the gas layer near the wall. The particles used in the previous studies were on the scale of a micrometer or larger. It is very likely that the motion of nanoparticles in the fluid will also enhance heat transfer. Therefore, more studies are needed on heat transfer enhancement in nanoparticle-fluid mixtures. Thermal conductivities of nanoparticle-fluid mixtures have been reported by Masuda et al. [26], Artus [27], and Eastman et

al. [28] adding a small volume fraction of metal or metal oxide powders in fluids increased the thermal conductivities of the particle-fluid mixtures over those of the base fluids.

The viscosity of nanofluids, which is one of the key influencing factor in heat transfer [29−31], has not received as much attention so far. The experimental and simulation results indicate that nanoparticle size is of crucially important to the viscosity of the nanofluid, as the nanoparticle size increases or changes. Although viscosity influences interfacial phenomena and flow characteristics, very few studies have been performed on the effective viscosity of nanofluids as a function of volumetric loading of nanoparticles [26-28]. The primary results from these studies indicate that the viscosity of a nanofluid increases with increasing nanoparticle volume fraction. In addition to the very few experimental studies have been carried out, few theoretical models are available for the prediction of the effective viscosity of nanofluids as a function of temperature and particle volume fraction. But they lack in consistency. It is worthwhile to study temperature-dependent viscosity of nanofluids for their potential applications especially in nanofluidic systems.

2.3 Nanofluids Preparation and Characterization

2.3.1 Preparation

Preparation of nanofluids is the first key step in experimental studies with nanofluids. Nanofluids are not simply liquid-solid mixtures. Some special requirements are essential e.g. even and stable suspension, durable suspension, negligible agglomeration of particles, no chemical change of the fluid, etc. Nanofluids are produced by dispersing nanometer scale solid particles into base liquids such as water, ethylene glycol (EG), oils, etc. There are mainly two techniques used to produce nanofluids.

1. Single-step method
2. Two-step method

Single Step Method: The single step direct evaporation approach was developed by Akoh et al. [32] and is called the VEROS (Vacuum Evaporation onto a Running Oil Substrate) technique. The original idea of this method was to produce nanoparticles, but it is difficult to subsequently separate the particles from the fluids to produce dry nanoparticles. A modified VEROS process was proposed by Wagener et al. [33]. They employed high pressure magnetron sputtering for the

preparation of suspensions with metal nanoparticles such as Ag and Fe. Eastman et al. [34] developed a modified VEROS technique, in which Cu vapour is directly condensed into nanoparticles by contact with a flowing low-vapor-pressure liquid (Ethylene Glycol). A vacuum-SANSS (submerged arc nanoparticle synthesis system) method has been employed by Lo et al. [35] to prepare Cu-based nanofluids with different dielectric liquids such as de-ionized water, with 30%, 50%, 60% volume solutions of ethylene glycol and pure ethylene glycol. Different morphologies, which are obtained, are mainly influenced and determined by the thermal conductivity of the dielectric liquids. CuO, Cu_2O, and Cu based nanofluids also can be prepared by this technique. An advantage of the one-step technique is that nanoparticle agglomeration is minimized, while the disadvantage is that only low vapor pressure fluids are compatible with such a process. Recently, a Ni nanomagnetic fluid was also produced by Lo et al. [36] using the SANSS method.

Two-step process: C.G. Granqvist, and R.A. Buhrman [37] found the two- step process. In this firstly, nanoparticles are produced as a dry powder, typically by inert gas condensation. The second step involves dispersion of dry nanoparticle powder into a base fluid, like water, oil or ethylene glycol. Romano et al [37] reported an advantage of the two-step process is that the inert-gas condensation technique has been scaled up to commercial nanopowder production. A deficiency of this method is the tendency of nanopowder to agglomerate during storage and dispersion in the base fluids, particularly with heavier metallic nanoparticles. Surfactants and other surface-stabilization additives can be used to achieve more homogeneous and more stable suspensions. In addition to mechanical mixing, ultra-sonic mixers can be used to break up agglomerates and give more uniform dispersions.

2.3.2 Characterization

Imaging analysis of nanofluids is done using electron microscope (SEM/TEM, TEM being preferred over SEM for nanofluids) and most of the reported studies makes use of TEM for characterizing nanofluids. Cryogenic transmission electron microscopy might provide a powerful characterization method, but few laboratories are equipped to apply this technique. Scanning probe microscopy (SPM) has not found much use for characterizing nanofluids. A simplistic approach makes use of particle size analyzer based on dynamic light scattering (DLS). Robert J.

Hunter [38] has used DLS systems for particle size distribution to augment the results with TEM as main characterization tool. A valuable characterization tool for the structure of suspensions at nanoscale is the small angle x-ray scattering (SAXS) and small angle neutron scattering (SANS). In these techniques a nanofluid is illuminated by a collimated x-ray or neutron beam and the intensity of scattering is measured as a function of angle. Lurio et al. [39] measured equilibrium dynamics by using a relatively recent x-ray scattering technique called x-ray photon correlation spectroscopy (XPCS), which is based on the traditional laser based photon correlation spectroscopy (PCS). In the XPCS technique a sample is illuminated with a fully coherent x-ray beam; instead of the more typical situation in which the incident x-rays consist of a large number of incoherent regions. The effect of coherent illumination is to obtain a speckle pattern superimposed on the usual SAXS pattern.

2.4 Factors Effecting Viscosity of Nanofluids

There are many factors (particle size and shape, temperature, volumetric concentration, sonication time, viscosity of base fluid etc.) which effects the viscosity of nanofluids. The detail of these factors are as given below:

Praveen *et al.* [40] measured the viscosity of copper oxide nanoparticles dispersed in ethylene glycol and water. An LV DV-II+ Brookfield programmable viscometer was used for the viscosity measurement. They used CuO nanoparticles with an average diameter of 29 nm and the particle density of 6.3 g /cc. The particles were dispersed in a 60:40 (by weight) ethylene glycol and water mixture, to prepare nanofluids with different volume concentrations (1, 2, 3, 4, 5, and 6.12%). The viscosity measurements were carried out in the temperature range of -35 to 50°C. The variation of the shear stress with shear strain was found to be linear for a 6.12% concentration of the nanofluid at -35°C, which confirmed that the fluid has a Newtonian behavior. The results of the experiment are as shown in fig. 2.1 below and it shows at all concentrations, the viscosity value was found to be decreasing with an increase in the temperature and a decrease in concentration of the nanoparticles.

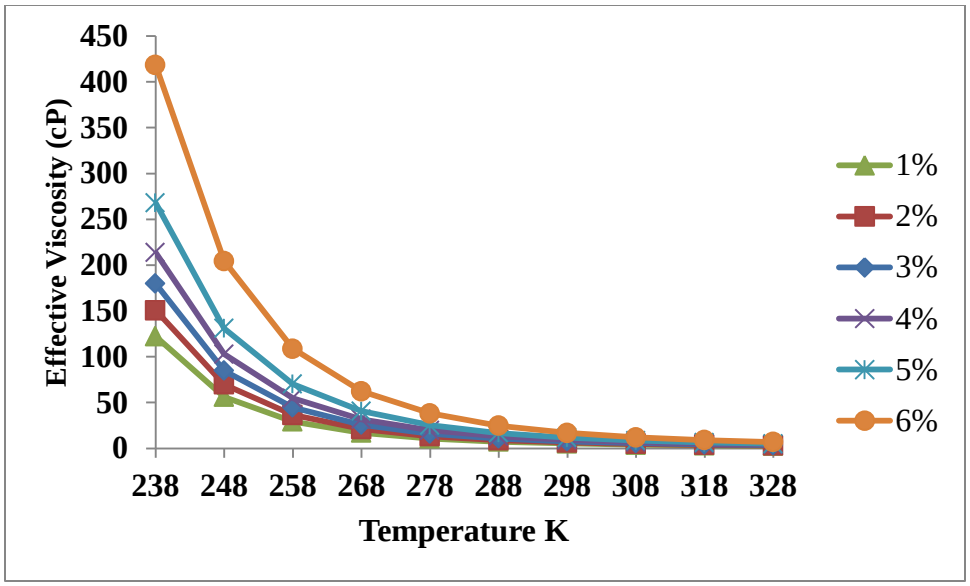

Fig.2.1 Effective viscosity v/s temperature (K) at different volumetric concentrations

Nguyen *et al*. [41] measured the temperature and particle size dependent viscosity of Al_2O_3-water and CuO water nanofluids. The average particle sizes of the samples of Al_2O_3 nanoparticles were 36 and 46 nm, and that of CuO nanoparticles was 29 nm. The viscosity was measured using a Visco Lab 450 Viscometer (Cambridge Applied Systems, Massachusetts, USA). The dynamic viscosities of nanofluids were measured for fluid temperatures ranging from 22 to 65°C, and particle volume fractions varying from 1 to 9.4%. Both Al_2O_3-water and CuO-water nanofluids showed an increase in the viscosity with an increase in the particle concentration, the largest increase being for the CuO-water nanofluid. The alumina particles with 46 nm were found to enhance viscosity more than the 36 nm nanoparticles.

At 12% volume fraction, the 46 nm particles were found to enhance the viscosity 5.25 times, against a 3% increase by the 36-nm particles. The results are as shown in fig 2.2. The increase in the viscosity with respect to the particle volume fraction has been interpreted as due to the influence on the internal shear stress in the fluid. The increase in temperature has shown a decrease in the viscosities for all nanofluids, which can be attributed to the decrease in inter-particle and inter-molecular adhesive forces.

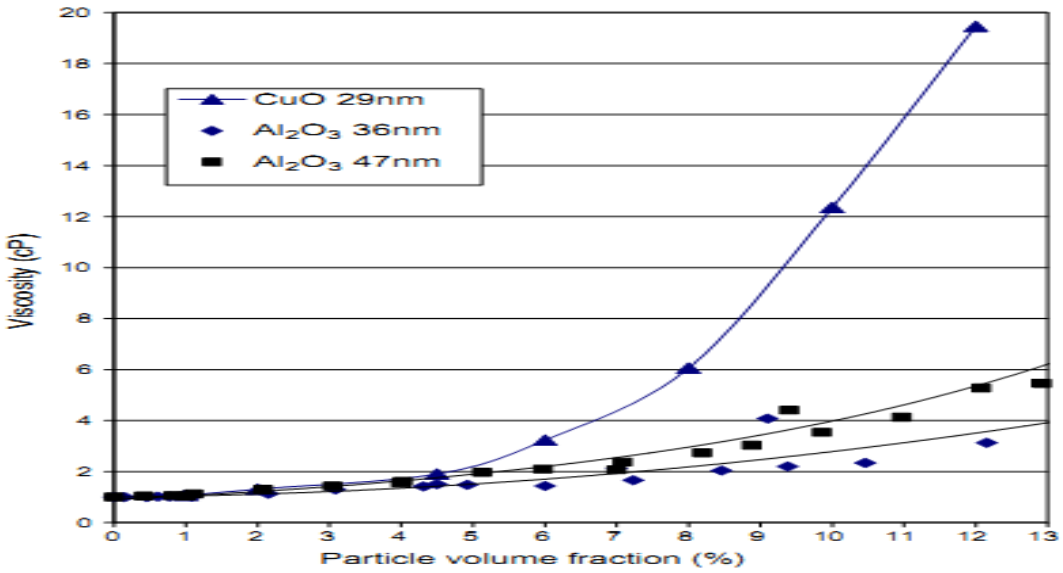

Fig. 2.2 Viscosity v/s partial volume fraction for CuO and Al_2O_3 with different diameters

Nguyen *et al*. [41] made an experimental model. The graphical representation of experimental model is as shown in fig. 2.3. And it represents the increase in the viscosity of the CuO-H_2O based nanofluid with the increase in the volumetric concentration.

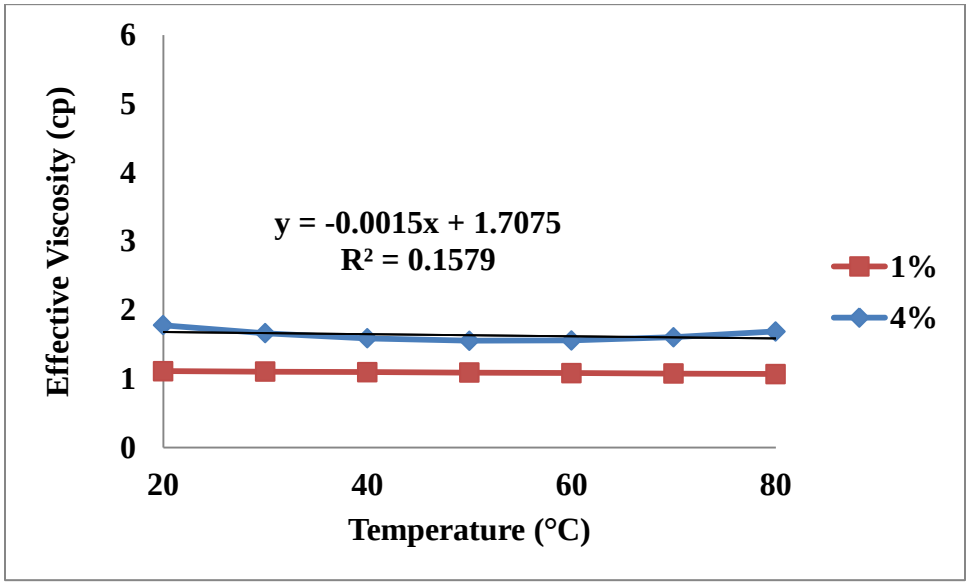

Fig. 2.3 Effective viscosity v/s temperature for different volumetric concentration

Kulkarni *et al.* [42] investigate the viscous behavior of CuO-H_2O solution in which volumetric concentration is in between 0.05 to 0.15 and made the diameter of the particle 29nm. From the experiment it found that the viscosity of the nanofluid increase as the volumetric concentration

increases. At 0.12 percent of the volumetric concentration, at 268K the viscosity came to 56 centipose.

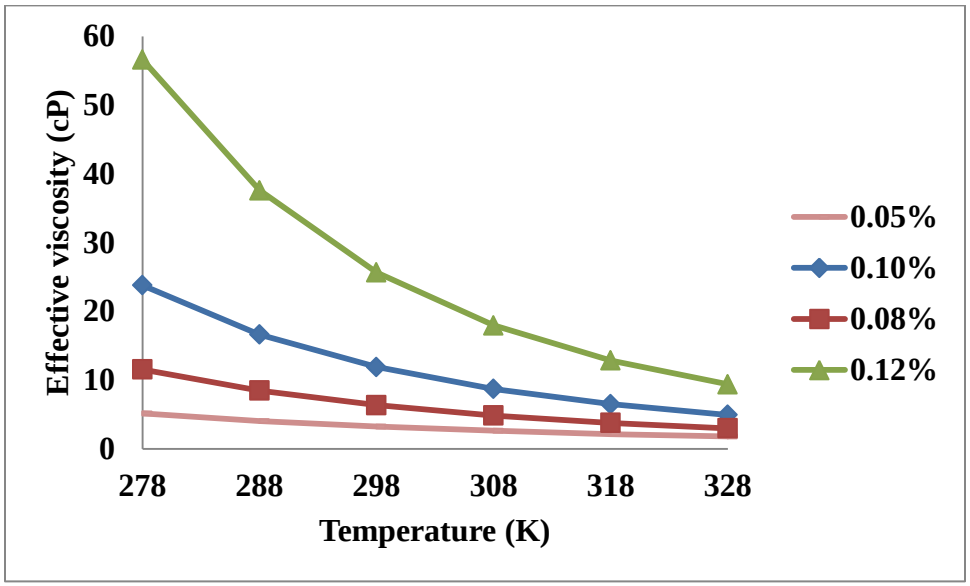

Fig. 2.4 Effective viscosity v/s Temperature for different volumetric concentrations

Namburu *et al.* [43] investigated the viscosity of silicon dioxide (SiO_2) nanoparticles with various diameters (20, 50 and 100 nm) suspended in a 60:40(by weight) ethylene glycol and water mixture. Nanofluids with particle volume percentages ranging from 0 to 10% were examined. Viscosity experiments were carried out over wide temperature ranges, from -35^{o}C to 50 ^{0}C, to demonstrate their applicability in cold regions.

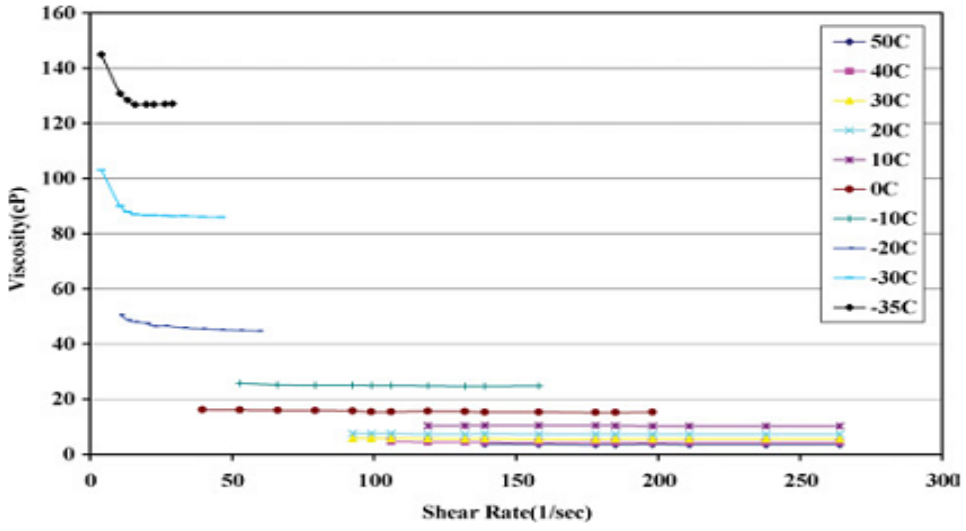

Fig.2.5 Viscosity of the silicon dioxide nanofluid (50 nm) with 6% volume concentration against shear rate for varying temperatures from -35 to 50 ^{0}C [43]

As shown in the fig. 2.5, the curves between viscosity and shear rate are horizontal straight lines for temperatures more than -10 ^{0}C; this clearly demonstrates that silicon dioxide nanofluids display Newtonian behavior. For the temperatures below -10 ^{0}C, the nanofluids demonstrate non-Newtonian behavior as the curves are nonlinear and the viscosity varies with shear rate.

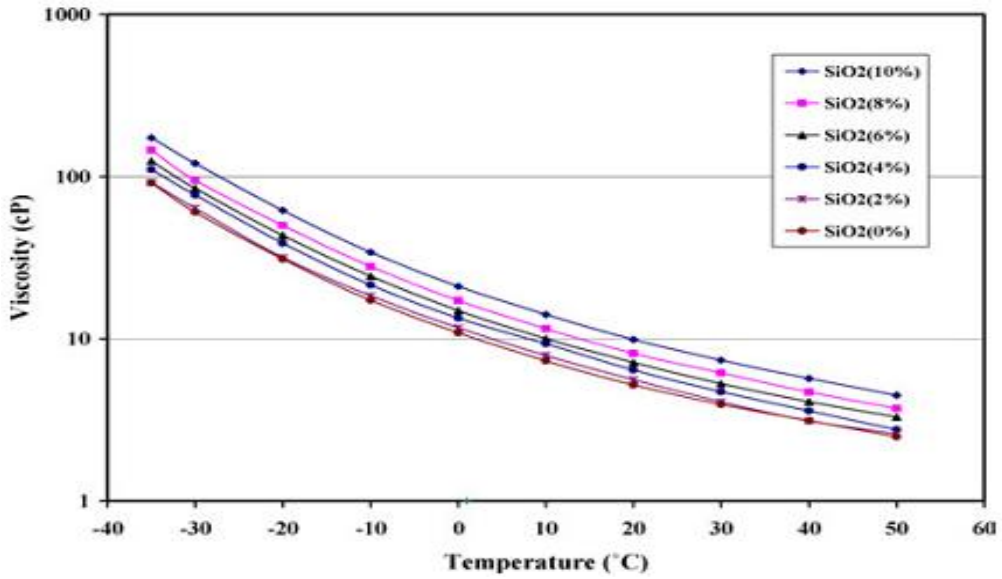

Fig.2.6 Experimental values of viscosity for varying volume concentrations of silicon dioxide nanofluids (50 nm) with respect to temperature [43]

It was indicated in Fig. 2.6 indicates that viscosity diminishes exponentially as the sample fluid temperature increases. Furthermore, it shows that with higher nanoparticle concentrations, nanofluids possess higher viscosity. The shape of each curve for different concentrations of nanofluids in fig. 2.6 is similar, which indicates the consistency of trend of the experimental measurements. Similar trends were observed for viscosity measurements of silicon dioxide nanofluids with nanoparticle diameters of 20 and 100 nm.

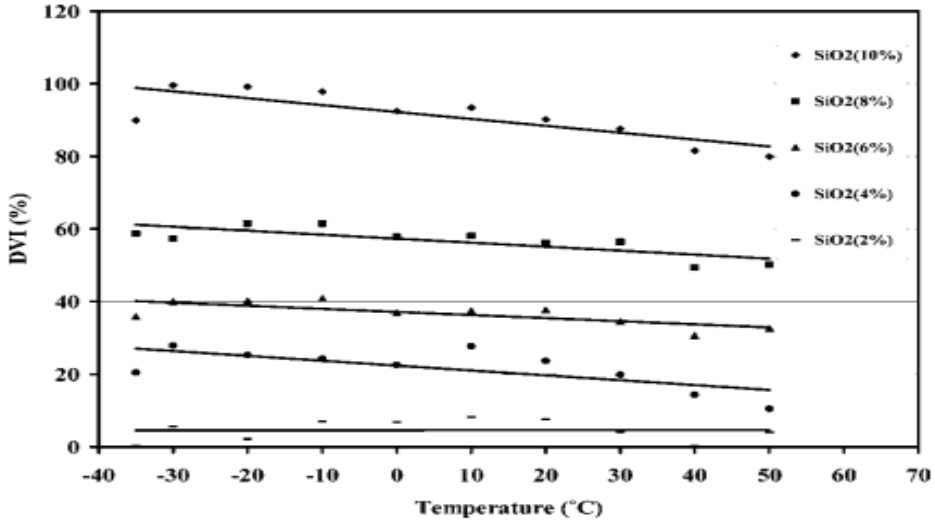

Figure 2.7 DVI against temperature for varying concentrations of silicon dioxide nanofluids (50 nm) [40]

The DVI is defined as the ratio of difference between the nanoparticles suspension viscosity and the viscosity of base fluid to the viscosity of base fluid.

From Fig. 2.6, we infer that the DVI reduces from -35 to 50 ^{0}C,for all nanofluid concentrations. If the concentration of nanoparticles is low, the DVI will be low as well.

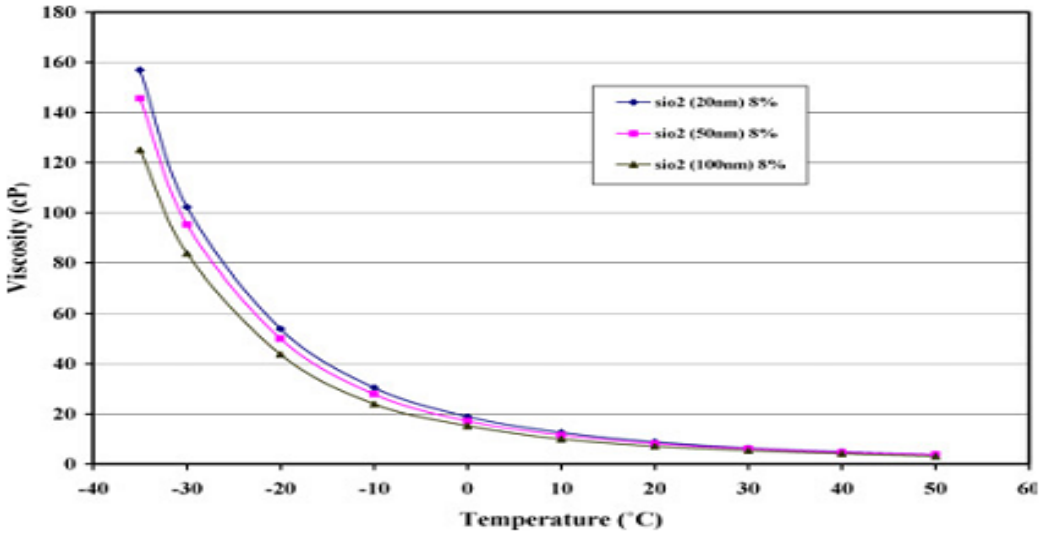

Fig.2.8 Effect of silicon dioxide nanoparticle diameter on nano-fluid viscosity for varying temperature. [43]

From Fig. 2.8, we infer that for the same volumetric concentration of 8%, silicon dioxide nanofluids with highest nanoparticle diameter 100 nm have the lowest viscosity. Similar trends of experimental results were obtained for all concentrations of silicon dioxide nanofluids.

Ravi Prasher *et al*. [44] performed the experiments and give results on the viscosity of alumina based nanofluids which are reported for various shear rates, temperature, nanoparticle diameter, and nanoparticle volume fraction. From the data it seems that the increase in the nanofluid viscosity is higher than the enhancement in the thermal conductivity as reported in the literature. It is shown, however, that the viscosity has to be increased by more than a factor of 4-relative to the increase in thermal conductivity to make the nanofluid thermal performance worse than that of the base fluid. But still there is great advantage in using nanofluids.

Le-Ping Zhou *et al* [45] investigated that the specific heat capacities of nanofluids were different from that of base fluid and vary with the size and volume concentration of nanoparticles. The specific heat capacity of CuO nanofluid decreases gradually with increasing volume concentration of nanoparticles. In most of the cases, however, there are no experimental data available for specific heat capacity, such that two kinds of models have been generally adopted to deduce it from the value of base fluid and nanoparticles. One is macroscopic, that the specific heat capacity of a nanofluid is equal to the volume average of the specific heat capacities of base fluid and nanoparticles. The other is microscopic, which assumes the base fluid and the nanoparticles are in their thermal equilibrium, respectively. Using the volumetric heat capacity instead, the volumetric heat capacity of a nanofluid can be expressed as the sum of the volumetric heat capacities for base fluid and nanoparticles, using their respective volume concentrations.

Sheng-Qi Zhou and Rui Ni [46] investigate the specific heat cp of water-based Al_2O_3 nanofluid with a differential scanning calorimeter. The result indicates that the specific heat cp of nanofluid decreases gradually as the nanoparticle volume fraction increases from 0.0% to 21.6%. The relationship between them exhibits good agreement with the prediction from the thermal equilibrium model. The other simple mixing model fails to predict the specific heat of nanofluid.

Table 2.1 illustrates a summary of the effective viscosity data reported by various research groups.

Table 2.1

Sr no.	**References**	**Nanoparticl-es used**	**Basefluid**	**Concentr-ation**	**Temperat-ure Range**	**Percentage enhancement in viscosity**
1.	Praveen *et al.* [44]	CuO (29 nm)	60:40 (in weight) ethylene glycol and water mixture	1, 2, 3, 4, 5, 6.12%	-35 to 50°C	For 6.12% conc: 4.5 times @ 35°C and 3 times @ 50°C
2.	Nguyen *et al.* [52,45]	CuO (29 nm) Al_2O_3(36 and 46 nm)	Water	1-12%	22 to 65°C	CuO @ 9%: 6-10 times Al_2O_3(36 nm) @ 9%: 4.5-3.5 times Al_2O_3(46 nm) @ 9%: 5.4-4.4 times
3.	Chen *et al*. [46]	Titanate nanotubes (diameter approx. 10 nm, length approx. 100 nm, aspect ratio approx. 10)	Ethylene glycol	0.5, 1.0, 2.0, 4.0, and 8.0% by weight	20-60° C	@ 8%: High shear viscosity is in the range of 10-35 m Pa s
4.	Phuoc *et al*. [47]	Fe_2O_3 (20-40 nm)	Deionized water containing 0.2% polymer by weight	1, 2, 3, 4%	25°C	@ 2%: Infinite viscosity is 12.25 cP for 0.2% PEO (Polyethylene oxide)

			as a dispersant			surfactant, and 2.58 cP for 0.2% PVP (Polyvinylpyrrolidone) surfactant
5.	Garg *et al*. [48]	MWCNT (multi-walled carbon nanotube) (diameter of 10-20 nm, length of 0.5-40 μm)	Deionized water with 0.25% by mass of gum Arabic	1% by mass	15 and 30°C	Viscosity of nanofluids increases with sonication time. Beyond a critical sonication time it decreases due to increased breakage of CNTs
6.	Murshed *et al.* [49]	TiO_2 (15 nm)/Al_2O_3 (80 nm)	Deionized water with Cetyl Trimethyl Ammonium Bromide (CTAB) surfactant (0.1 mM	1-5% by volume	-	@ 5% of Al_2O_3 viscosity increases by 82% @ 4% of TiO_2 viscosity increases by 82%
6.	Chena *et al*. [50]	TiO_2 (25 nm) and TNT (Titanate nanotubes) (diameter approx. 10 nm, length	Water, ethylene glycol	0.1-1.8% by volume	-	@ 0.6% of water-TNT 80% increase in viscosity @ 1.8% EG-TNT 60% increase in viscosity

		approx. 100 nm, aspect ratio approx. 10)				@1.8% EG-TiO2 20% increase in viscosity
8.	Duangthongsuk *et al*. [53]	TiO_2 (21 nm)	Water	0.2, 0.6, 1.0, 1.5, and 2.0% with pH values of 6.5, 6.1, 6.0, 6.8, and 6.5,	15, 25 and 30°C	@ 15°C for the conc. range of 0.2-2% viscosity increases by 4-15%.
9.	Lee *et al*. [51]	Al_2O_3 (30 ± 5 nm)	Deionized water (DI)	0.01-0.3 vol.%	21-39°C	@ 21°C for the conc. range of 0.01-0.3% viscosity is enhanced by 0.08-2.9%

2.5 Viscosity Models for Nanofluids

There are number of fundamental models used to predict the viscous behaviour if nanofluid. Few of them are listed here. Einstein [13] was the first who determines the effective viscosity of the suspension of the spherical particles as a function of volume fraction(volume fraction less than 5%). The equation was developed by using phenomenological hydrodynamic equations. This equation was expressed by:

$$\mu_{eff} = \mu_f \left(1 + \frac{5}{2}\emptyset\right) \quad (1)$$

Since Einstein's analysis of the viscosity of a dilute suspension of rigid spheres in a viscous liquid, several equations have been developed in an effort to extend Einstein's formula to suspensions of higher concentrations, including the effect of non-spherical particle concentrations [15-19]. For example, Brinkman [15] presented a viscosity correlation that extended Einstein's equation to concentrated suspensions:

$$\mu_{eff} = \frac{1}{(1-\emptyset)^{2.5}} = (1+2.5\emptyset + 4.365\emptyset^2 \pm - - -)\ \mu_f \quad (2)$$

The effect of Brownian motion on the effective viscosity in a suspension of rigid spherical particles was studied by Batchelor [16]. For isotropic structure of suspension, the effective viscosity was given by:

$$\mu_{eff} = (1 + 2.5\emptyset + 6.2\emptyset^2)\ \mu_f \quad (3)$$

Lundgren [17] proposed the following equation under the form of a Taylor series in $\emptyset$:

$$\mu_{eff} = \frac{1}{1-2.5\emptyset}\mu_f = (1 + 2.5\emptyset + 6.25\emptyset^2 + 0(\emptyset^3))\ \mu_f \quad (4)$$

It is obvious that if the terms $0(\emptyset^2)$and higher are neglected, the above correlation reduces to that of Einstein.

Table 2.2 summarizes the commonly used models and correlations to predict the viscous behaviour of nanofluid.

Table 2.2 Summary of commonly used models

Models	**Effective Viscosity**	**Physical Model**	**Remarks**
Einstein [13]	$\mu_{eff} = \mu_f \left(1 + \frac{5}{2}\emptyset\right)$	-Based on the phenomenological hydrodynamic equations -Considered a suspension containing n solute particles in a total volume **V**	-Infinitely dilute suspension of spheres (no interaction between the spheres) - Valid for relatively low particle

			volume fraction
Brinkman [15]	$\mu_{eff} = \frac{1}{(1-\emptyset)^{2.5}} = (1+2.5\emptyset + 4.365\emptyset^2 \pm - -) \mu_f$	- Based on Einstein model - Derived by considering the effect of the addition of one solute-molecule to an existing solution	-Spherical particles - Valid for high moderate particle concentrations -Used Einstein's factor: (1 + 2.5∅)
Batchelor [16]	$\mu_{eff} = (1 + \eta\emptyset + K_H\emptyset^2)\mu_f = (1 + 2.5\emptyset + 6.2\emptyset^2)\mu_f$	–Based on reciprocal theorem in Stokes flow problem to obtain an expression for the bulk stress due to the thermodynamic forces – Incorporated both effects: hydrodynamic effects and Brownian motion	– Rigid and Spherical particles – Brownian motion – Isotropic structure – Huggins coefficient: K_H = 6.2 (5.2 from hydrodynamic effects and 1.0 from Brownian motion)
Lundgren [17]	$\mu_{eff} = \frac{1}{1-2.5\emptyset}\mu_f = (1 + 2.5\emptyset + 6.25\emptyset^2 + - - -))\mu_f$	– Based on a Taylor series expansion in terms of ∅	– Dilute concentration of spheres – Random bed

			of spheres
Graham [18]	$\mu_{eff} = (1 + 2.5\emptyset\ \ )\mu_f + \left[\frac{45}{\left(\frac{h}{r_p}\right)\left(2 + \frac{h}{r_p}\right)(1 + {}^{h}/_{r_p})^2}\right]\mu_f$	– A cell theory was used to derive the dependence of the zero-shear-rate viscosity on volume concentration for a suspension of uniform, solid, neutrally buoyant spheres – Based on Cage model of liquids and solutions	
Mooney [20]	$\mu_{eff} = \exp\left(\frac{25\emptyset}{1 - K\emptyset}\right)\mu_f = \{1 + 2.5\emptyset + [3.125 + (2.5K)\emptyset^2 + - - -\}\mu_f$ $1.35 < K < 1.91$	–Einstein's viscosity equation for an infinitely dilute suspension of spheres was extended to apply to a suspension of finite concentration – Based on first-order interaction between particles (crowding effect)	– Rigid spherical spheres –Mono disperse suspension of finite concentration – Not valid at high concentrations – Considered the volume fraction of a suspension to be divided into two portions

Eilers [21]	$\mu_{eff} = \mu_f \left[\frac{1.25\emptyset}{1-\emptyset \ /0.68}\right]$=(1 + 2.5∅ $+ 4.65\emptyset^2 + ----)\mu_f$	– Based on experimental data	– Suspensions of bitumen spheres –Curve fitting of the experimental data
Saito [22]	$\mu_{eff} = \left(1 + \frac{2.5}{1-\emptyset}\emptyset\right)\mu_f$ $= (1 + 2.5\emptyset + 2.5\emptyset^2 + ---)\mu_f$	– Developed based on a theory for spherical solute-molecules in which a single solute molecule is placed in the field of flow, obtained by averaging over all the possible positions of a second solute-molecule	– Spherical rigid particles – Brownian motion – Very small particles

The graphical representation of all the theoretical models are as shown in fig.1 below.

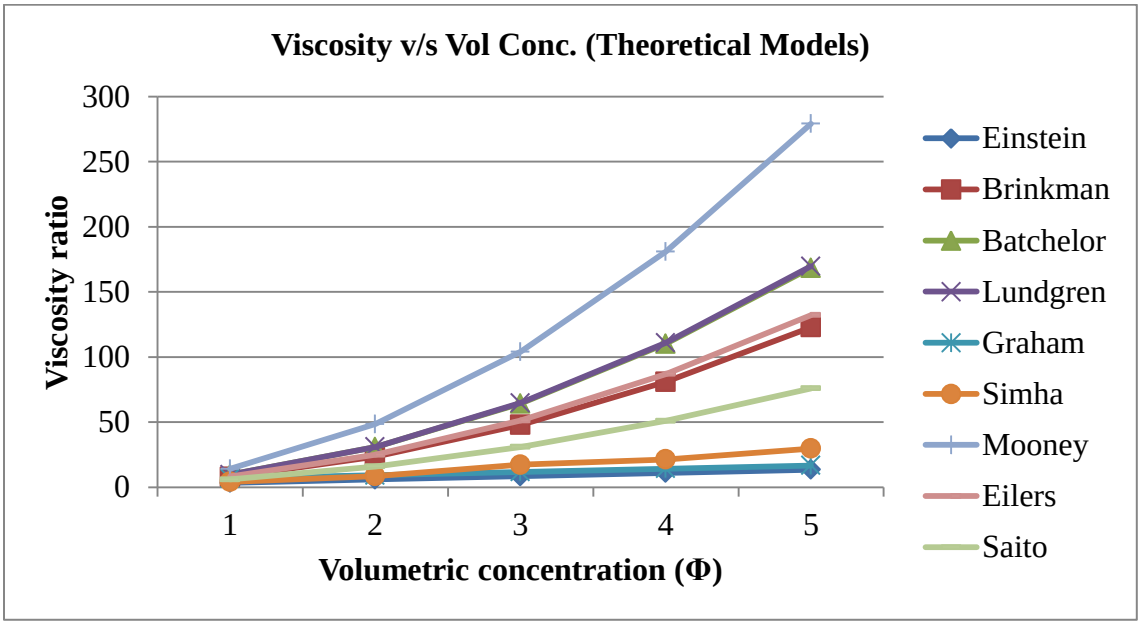

Fig. 2.9 Viscosity ratio v/s volumetric concentration

The Einstein's model is based on the phenomenological hydrodynamic equation and is valid only for spherical particles with relatively low volume fraction. The brinkman's model is based on the Einstein's model. The Batchelor consider both the hydrodynamic effect and the Brownian motion in his model. The Lundgren's model is the expansion of Taylor's series and consider dilute concentration of spherical particles. In Graham's model cell theory was used to derive the dependence of the zero-shear-rate viscosity on volume concentration for a suspension of uniform, solid, neutrally buoyant spheres. Due to the cell theory the viscosity ratio of this model is more than the other models. These models are mainly used to predict the nanofluid viscosity variation with change in volumetric concentration.

2.6 Objective

The literature review carried out in this chapter highlights about nanofluids, its preparation and characterization and thermophysical properties along with their applications in heat transfer area. As it has been observed that nanofluid can play a major role in various area of heat transfer technologies due to unique characteristics. Also work has been reported lacks in consistency and does not predict the complete behaviour of nanofluid. Fundamental models under estimate the viscosity and hence cannot be used to predict the viscosity of nanofluids. Above all shows that still a lot of investigations are needed to know the behaviour of nanofluid.

Based upon detailed literature survey following objectives are formulated:

1. Synthesis of CuO nanoparticles.
2. Characterization of CuO nanoparticles.
3. Preparation of nanofluid of volumetric concentration (0.005%, 0.05%, 0.01%, 0.1%) by Ultra sonicator (Oscar Ultra sonicator)
4. To investigate the viscous behaviour of CuO-H_2O, EG(ethylene glycol) based nanofluid at different temperatures (20^oC to 50^oC)
5. To study the shear thinning/ shear thickning of nanofluids.

CHAPTER 3

SYNTHESIS AND CHARACTERIZATION

3.1 Synthesis

Nanostructured materials present great promise and opportunities for a new generation of materials with improved properties for applications in sensors, optoelectronics, separation and catalysis. Catalysts, for example, are mostly nanoscale particles, and catalysis is a nanoscale phenomena [54-55]. Up to now, significant progress has been made in controlling the size of nanoscale materials and in understanding their unique size-dependent catalytic properties [56–59]. Meanwhile, controlling the shape of nanoparticles is an equally important aspect of desired catalyst synthesis [59–64]. It is known that the reactivity depends on the crystal plane of the catalyst for structure-sensitive reactions [75–68].

One would expect catalysis to be greatly dependent on the nanocrystallite shape used, since different nanocrystallites with different shapes expose different crystal planes [69]. Copper oxide is one of the most important catalysts, and is widely used in environmental catalysis. For carbonmonoxide oxidation, CuO catalysts may even substitute the noble metal catalysts because of their high catalytic activity [71-72]. Previous studies indicate that this reaction is an apparent structure sensitive process and the surface lattice oxygen of CuO is involved during the reaction [73-74]. Thus, the nature of the metal oxide surface should be of paramount importance. In recent years, the shapecontrolled synthesis of nanostructured CuO has attracted considerable attention [75-79].

In the present work, large scales of CuO nanoplatelets were synthesized through a facile softer synthetic route, which involved the precipitation of copper salts with concentrated NaOH solutions at room temperature.

3.2 Experimental Details

CuO nanoplatelets.

$Cu(CH3COO)_2 \cdot H_2O$ (3.0 g) was dissolved in distilled water, and appropriate amounts of concentrated NaOH solution were rapidly added under stirring in a Teflon flask at room

temperature. The black precipitate appeared quickly, indicating the formation of CuO. The final NaOH is about 5 M. The resultant product was then aged together with mother liquor at room temperature for 5 h. The final product was collected by filtration, and washed with deionized water to remove any possible ionic remnants, and then dried at 60 ◦C and calcined at 350 ◦C for 4 h.

3.3 Results and Discussion:

After the synthesis part, for the verification of material is done by using XRD at Panjab University, Chandigarh. And the result of XRD is shown below:

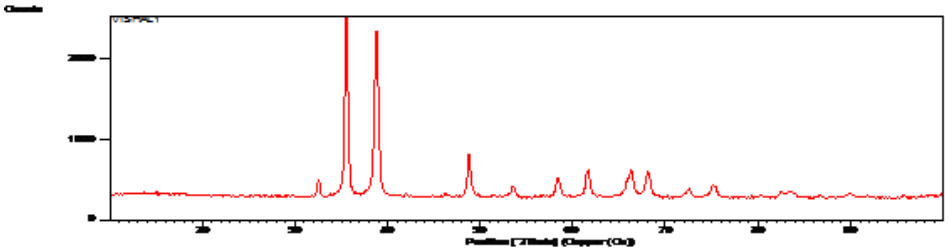

Fig. 3.1 XRD results

The XRD shows the various peaks and for CuO the peaks are always in between 30^{o} to 40^{o}.So from XRD it come to know that the particles are CuO in nature.

The verification of size of particles is done by using SEM available Thapar University, Patiala.

The results of SEM are as shown in fig 3.2 and 3.3below:

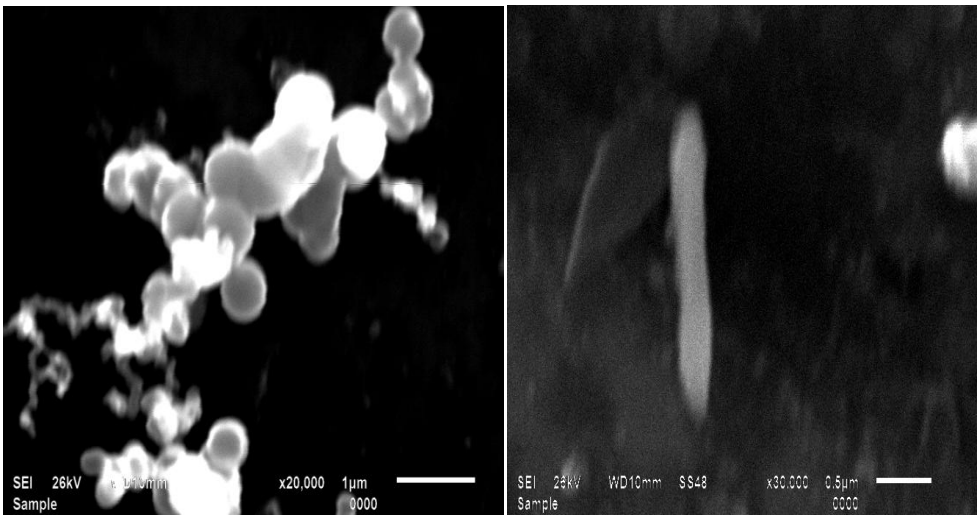

Fig 3.2 SEM Image **Fig 3.3 SEM Image**

From figures we infer the shape of the platelets is not clear and also size is in the microscale. So, it was an attempt in the synthesis of CuO platelets, but unfortunately were not synthesized in proper shape and size. But the reaction was accurate and the cleared from XRD result. There need precision of temperature, time in the synthesis of nanoparticles.

3.4 Characterization

Characterization and reporting are fundamental to science. Measurement is characterization, the language of science. Measurement is accomplished with the tools: the instruments, machines, equipment and computer hardware and software. There are many types of characterization methods and more predate the advent of nanoscience and nanotechnology.

3.5 Different Methods of Characterization

There are many methods for the characterization of the nanofluids which are as given below in the following tables [88]

Table 3.1 Optical (Imaging) Probe Characterization Methods

Acronym	Technique	Analytical Value
	Binocular Microscopes Compound Microscopes	Imaging/gross morphology Imaging/fine morphology
CLSM SNOM 2PFM	Confocal laser-scanning microscope Scanning near-field optical microscopy Two-photon fluorescence microscopy	Imaging/ ultrafine morphology Rastered images Fluorophores/biological samples
DLS PCS QELS	Dynamic light scattering Photon correlation spectroscopy	Particle sizing

	Quasi-elastic light scattering	
BAM	Brewster angle microscopy	Gas-liquid interface imaging

Table 3.2 Electron Probe Characterization Methods

Acronym	**Technique**	**Analytical Value**
SEM	Scanning Electron Microscopy	Raster imaging/topology morphology
EPMA	Electron Probe microanalysis	Particle size/local chemical analysis
TEM	Transmission electron microscopy	Imaging/ particle size-shape
HRTEM	High-resolution transmission electron microscopy	Imaging structure chemical analysis
STEM	Scanning transmission electron microscopy	Biological samples
FEM	Field emission microscopy	Surface structure/molecular properties
	Electron diffraction	Crystal structure
RHEED	Reflection high energy electron diffraction	Surface structure
LEED	Low-energy electron diffraction	Surface/adsorbate bonding
EBSD	Electron backscatter diffraction for SEM	Crystallographic information
EELS	Electron energy loss spectroscopy	Inelastic electron interaction

AES	Auger electron spectroscopy	Chemical surface analysis
EBIC	Electron beam induced current	Transport properties in semiconductor

Table 3.3 Scanning Probe Characterization Methods

Acronym	**Technique**	**Analytical Value**
AFM	Atomic force microscopy	Topology/imaging/surface structure
LFM	Lateral force microscopy	Surface/friction analysis
CFM	Chemical force microscopy	Chemical/surface analysis
MFM	Magnetic force microscopy	Magnetic materials analysis
STM	Scanning tunneling microscopy	Topology/surface structure/imaging
STS	Scanning tunneling spectroscopy	Electronic density of states
APM	Atomic probe microscopy	Three-dimensional imaging
FIM	Field ion microscopy	Chemical profiles/atomic spacing
IAP	Imaging atomic probe	Emitted ions for imaging surface
APT	Atomic probe tomography	Position-sensitive lateral location of atoms
POSAP	Positive-sensitive atomic probe	Mass position resolution

Table 3.4 Photon (Spectroscopic) Probe Characterization Methods

Acronym	**Technique**	**Analytical Value**
UPS	Ultraviolet photoemission	Surface analysis

	spectroscopy	
UVVS	UV-visible spectroscopy	Chemical analysis
AAS	Atomic absorption spectroscopy	
AES	Atomic emission spectroscopy	
	Fluorescence spectroscopy	Elemental analysis
ICP	Inductively coupled plasma spectroscopy	
FS		
SPR	Surface Plasmon resonance spectroscopy	Surface/adsorbate analysis
LSPR	Localized surface Plasmon resonance	Nanosized particle analysis
PLS	Photoluminescence spectroscopy	Elemental analysis
RS	Raman spectroscopy	Vibration analysis
SERS	Surface-enhanced Raman spectroscopy	Chemical analysis/bond structure
SERRS	Surface –enhanced resonant Raman spectroscopy	SERS coupled with electronic transition
XRD	X-ray diffraction	Crystal structure
XRF	X-ray fluorescence	
EDX	Energy-dispersive x-ray spectroscopy	Elemental analysis
WDS	Wavelength dispersive x-ray spectroscopy	

Table 3.5 Ion- particle Probe Characterization Methods

Acronym	**Technique**	**Analytical Value**
MS	Mass spectroscopy	Material composition

SIMS	Secondary ion mass spectroscopy	Composition of solid surface
RBS	Rutherford back scattering	Quantitative-qualitative elemental analysis
NSS	Neutron scattering spectroscopy	Chemical structure adsorbate bonding
SANS	Small angle neutron scattering	Surface characterization
NRA	Neutron reaction analysis	Depth profiling of solid thin films
PIXE	Particle-induced x-ray emission	Nondestructive elemental analysis

Table 3.6 Thermodynamic Characterization Methods

Acronym	**Technique**	**Analytical Value**
TGA	Thermal gravimetric analysis	Mass loss v/s temperature
	Differential thermal analysis	
DTA	Differential scanning	Reaction heats heat capacity
DSC	calorimetry	Reaction heats phase changes
TMA	Thermal mechanical analysis	Thermal mechanical properties
TPD	Temperature-programmed desorption	Surface adsorbate properties
TDS	Thermal desorption spectroscopy	Coupled with MS
SCAC	Single crystal absorption calorimetry	Absorption and adhesion energies
TL	Thermoluminescence	Surface states detrapping
BET	Brumauer-Emmett-Teller method	Surface area analysis
MP	Mercury porosimetry	Pore volume, pore size

BJH	Barnett-Joyner-Halenda method	Pore size distribution
Sears	Sears method	Colloid size, specific surface area

3.6 Types of characterization methods

Nanoscience and nanotechnology are interdisciplinary in nature. It is fair to say that an equally broad inventory of characterization and analytical techniques applies to nanostructured materials. There are approximately 600 single –signal characterization techniques and approximately 100 that are considered to be multisignal techniques [2]. These numbers are based on the types and combinations of three kinds of physical phenomena: (1) *primary* (1^o) analytical probes (electrons, photons, neutrons, ions etc) and input stresses (heat, pressure, electric field, magnetic field, electricity, mechanical stress etc.) (2) the types of measurable *secondary* effects (2^o) (electrons, electromagnetic radiation, heat, pressure, volume change, mechanical deformation etc.) and (3) the monitoring medium of choice (energy, temperature, mass, intensity, time, angle, or phase)[2]. The 1^o probe, whether electron or photon, interacts with matter. The matter then responds to regain its equilibrium state. During this process, the 1^o probe is modified. Exicited electrons, phonons, excitons or plasmons are some examples of how matter is altered. Alterations of the 1^o probe result in the 2^o effect- the signal we measure [2].

3.6.1 Optical Probe Characterization Techniques.

The primary probe in optical methods (table 1) is visible of wavelength within the 400 to 800 nm range. The 2^o signal from most 1^o photon methods is usually another photon. The 2^o photon signal arises from many possible physical phenomena, such as elastic scattering, inelastic scattering or from emission.

Human eyes have great depth of field and depth of foucs; however, they are not efficient at peering into nanostructured materials without assistance. Binocular scopes are useful for viewing gross morophology like a clump or large strands of carbon nanotubes. Compound microscopes offer more detail but resolution is limited to a few hundred microns. Confocal, near-field, and two-photon microscopes using visible and near ultraviolet (UV) 1^o photons have managed to

push the resolution envelope of optical methods into the sub-100 nm range. Dynamic light scattering is an optical technique that is used to measure particle size, and Brewster angle microscopy (BAM) is used to analyze phase behavior at an air-water interface. Brewster's law is given by

$$\theta_B = arctan\left(\frac{m_2}{m_1}\right) \quad (1)$$

Where m_2 and m_1 are the refractive indices of 2 media and is applicable to light that moves between those media and is applicable to light that moves between those media. θ_B is the Brewster's angle, the point at which light of one polarization cannot be reflected. Selected optical methods are listed in table 3.1. Optical characterization methods are used primarily for imaging but also useful in chemical analysis.

3.6.2 Electron Probe Characterization Methods

Electron probe characterization methods use high-energy beams. Electron beams are used for imaging, chemical analysis and determination of material structure. The most familiar electron probe methods are scanning electron microscopy (SEM) and transmission electron microscopy (TEM). In SEM, the electron beam is rastered across the analytical surface. A raster is a rectangular pattern of parallel scanned lines from which an image is assembled. Electron guns in older televisions produced a picture by rastering electrons over a phosphor grid. Electron probe methods are listed in table 3.2. SEM and TEM instruments are usually coupled to other types of analytical tools, primarily with energy-dispersive x-ray analysis.

3.6.3 Scanning Probe Characterization Techniques

All scanning probe microscopy (SPM) methods have two things in common: a finely sharpened probe tip and a system that enables the tip to scan over the surface of a sample. An image is acquired by moving the probe, or the sample, with a raster action-similar in concept with SEM but utilizing completely different types of probes. Resolution on the order of atoms is possible with scanning probe methods are listed in table 3.3.

3.6.4 Spectroscopic Characterization Methods

There are many kinds of 1^o photon probe techniques (Table 3.4). As in optical imaging, most photon probe methods involve a 1^o photon in and a 2^o photon out. UV-visible spectroscopy ,

based on absorption or emission of photon, is the most common form of spectroscopy. Although the wave length for UV-visible methods is within the nanoscale, the dimensions of most nanomaterials are much smaller. UV-visible techniques mainly involve electron transitions. Related parameters such as extinction, intensity, absorption, transmission, reflection and wavelength are measured during UV-visible spectroscopy. Raman and Fourier transform infrared spectroscopy are techniques that measure molecular and phonon vibrations of materials. In each case, 2^o photon carrier waves are analyzed and information about vibrational states is acquired. Symmetrical vibrations are exclusive to Raman spectroscopy and asymmetrical vibrations reside in the domain of infrared analysis. In surface Plasmon spectroscopy, the absorption of 1^o photons causes surface electron plasmons to oscillate. The wavelength, λ_{max} of the absorption is indicative of the surface state of the metal.

X-ray form another important category of 1^o photon excitation that is important to nanoscale analysis. The wavelength of x-rays ranges from 0.01 to 10 nm, corresponding quite well to the size of nanoparticles. The major 2^o effects ate photons or electrons depending on the type of the analyzer installed in the instrument. The two most *nanorelevent* x-ray techniques are x-ray diffraction (XRD) and energy-dispersive x-ray (EDX) which revels structural information and chemical analysis, respectively.

Nuclear magnetic resonance (NMR) and electron spin resonance (ESR) are techniques that rely on an applied magnetic field to induce signals. NMR is applicable to molecules that contain odd numbers of photons and neutrons. Electron paramagnetic resonance (EPR), commonly referred to as ESR, is a technique that is able to analyze materials that have unpaired electrons. There are numerous excellent sources that describe these techniques in more detail.

3.6.5 Ion –Particle Characterization Techniques

Mass spectroscopy (MS) involves the breakup of a parent particle into ionized components. Daughter particles are produced by electron impact and by other techniques. MS used to detect the presence of sodium nanoclusters in particle beams showed that cluster abundance was dependent on size; the most stable clusters possessed a *magic number* of atoms. Smalley and his group used MS to prove the existence of $C_{60.}$ Secondary ion MS (SIMS) is also popular method. Neutrons and ions are able to modify matter by inducing thermal vibrations, rupturing bonds and

displacing atoms. The 2^{o} signals comprise secondary ions. In addition, 1^{o} ion probes are capable of implantation and inducing ionization and de-excitation.

3.6.6 Thermodynamic Characterization Methods

Thermodynamic techniques are characterization methods that involve thermodynamic parameters. The primary probe is not a photon or an electron but rather a thermodynamic parameter such a temperature or pressure. In these cases, change in temperature, pressure, phase and volume are considered to be secondary effects. Bond energy, phase change, heat capacity, surface adsorption-desorption, volume change, surface tension and vapor pressure are some effects measured by thermodynamic techniques.

Thermoluminescence is a technique in which a photoluminescence response is generated in a material from heating. Thermoluminescence provide information about surface states- in particular, the ability to detect trapped metastable electron-hole pairs in nanoparticles. Heating the sample induces lattice vibrations that in turn provide energy for electron –hole recombination. Upon recombination, optical photons are emmited.

There are methods that have more “nano” relevance than others, but all apply with validity to nanomaterial characterization. The lists provided in table 1 through 6 are by no mean exhaustive. In general, two fundamental types of characterization exists: imaging by microscopy and analysis by spectroscopy. Other conventional techniques, like thermal gravimetric analysis (TGA) and the Brunauer- Emmett- Teller (BET) surface area methods, do not employ electromagnetic radiation per se but can be, in the very broadest of senses, considered to be spectroscopic methods because x and y axes are involved.

CHAPTER 4

INSTRUMENTS USED FOR EXPERIMENTAL WORK

4.1 **Ultrasonic processor/ Sonicator**

Sonication is the act of applying sound (usually ultrasound) energy to agitate particles in a sample, for various purposes. In the laboratory, it is usually applied using a probe known as a sonicator. Sonication is commonly used in nanotechnology to disperse nanoparticles in liquids.

Sonication can be used to speed dissolution, by breaking intermolecular interactions. It is especially useful when it is not possible to stir the sample. During the experiment, Oscar sonicator was used as shown in fig 4.1 below.

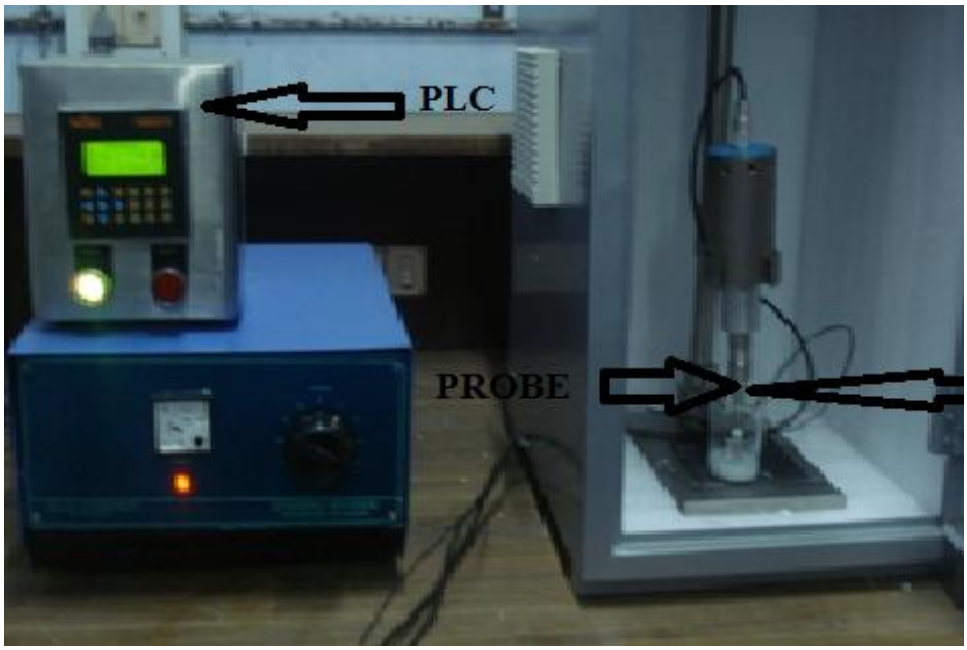

Fig 4.1 Ultra sonicator

The probe is immersed in the sample which is to be sonicated. The main specifications of the sonicator are as given below:

Specifications

Model	Processor SONOPROS PR-250 MP
Ultrasonic power	250 wats
Processing capacity	Upto 250 ml
Frequency	20± 3KHZ
Horn	1) Titanium horn 6mmØ 2) Titanium horn 12mmØ
Converter	PZT sandwich type OUC 116
Generator	Solid state, LOT type
Generator cabinet	MS powder coated
Stand base and pillar	SS 304

Power input	230V 50Hz, 3Amp
Converter	PZT sandwich type
Power variac	0-230V, 3Amp
Application	Particle dispersion

4.2 X-ray Powder Diffraction (XRD)

X-ray powder diffraction (XRD) is a rapid analytical technique primarily used for phase identification of a crystalline material and can provide information on unit cell dimensions. The analyzed material is finely ground, homogenized, and average bulk composition is determined.

4.2.1 Fundamental Principles of X-ray Powder Diffraction (XRD)

X-ray diffraction is a common technique for the study of crystal structures and atomic spacing. X-ray diffraction is based on constructive interference of monochromatic X-rays and a crystalline sample. These X-rays are generated by a cathode ray tube, filtered to produce monochromatic radiation, collimated to concentrate, and directed toward the sample. The interaction of the incident rays with the sample produces constructive interference (and a diffracted ray).

When conditions satisfy Bragg's Law ($n\lambda = 2d \sin\theta$). This law relates the wavelength of electromagnetic radiation to the diffraction angle and the lattice spacing in a crystalline sample. These diffracted X-rays are then detected, processed and counted. By scanning the sample through a range of 2θ angles, all possible diffraction directions of the lattice should be attained due to the random orientation of the powdered material. Conversion of the diffraction peaks to d-spacing allows identification of the mineral because each mineral has a set of unique d-spacing. Typically, this is achieved by comparison of d-spacing with standard reference patterns. Fig 4.2 shows the principal of XRD:

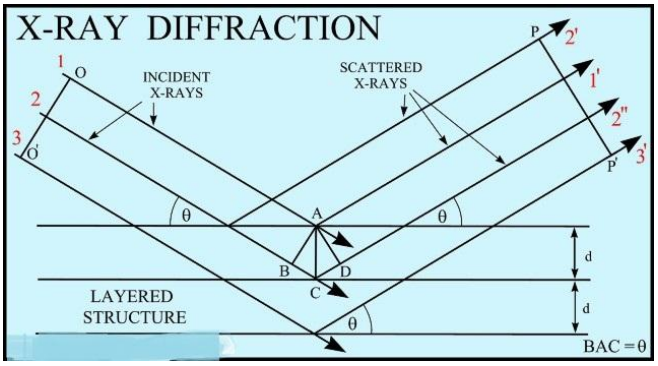

Fig. 4.2 X-Ray Diffraction

So, d= $\frac{n\lambda}{2\sin\theta}$

Brag's law, can be used to obtain the lattice spacing of a particular system through the following relationship:

d= $\frac{a}{\sqrt{h^2}+k^2+l^2}$

where a= lattice spacing

h, l & k are the miller indices.

4.3 Scanning Electron Microscope

Scanning Electron Microscope(SEM) uses electrons instead of light to form an image. The scanning electron microscope has many advantages over traditional microscopes. The SEM has a large depth of field, which allows more of a specimen to be in focus at one time. The SEM also has much higher resolution, so closely spaced specimens can be magnified at much higher levels. Because the SEM uses electromagnets rather than lenses, the researcher has much more control in the degree of magnification. All of these advantages, as well as the actual strikingly clear images, make the scanning electron microscope one of the most useful instruments in research today.

4.3.1 Working Of Scanning Electron Microscope

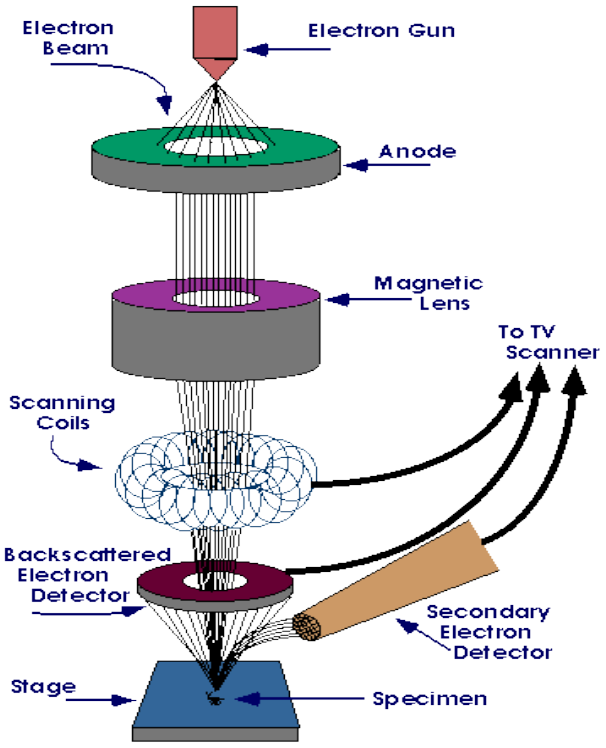

Figure 4.3 Scanning Electron Microscopy

As shown in fig. 4.3 the SEM is an instrument that produces a largely magnified image by using electrons instead of light to form an image. A beam of electrons is produced at the top of the microscope by an electron gun. The electron beam follows a vertical path through the microscope, which is held within a vacuum. The beam travels through electromagnetic fields and lenses, which focus the beam down toward the sample. Once the beam hits the sample, electrons and X-rays are ejected from the sample as shown in fig. 4.3. Detectors collect these X-rays, backscattered electrons, and secondary electrons and convert them into a signal that is sent to a

screen similar to a television screen. This produces the final image.

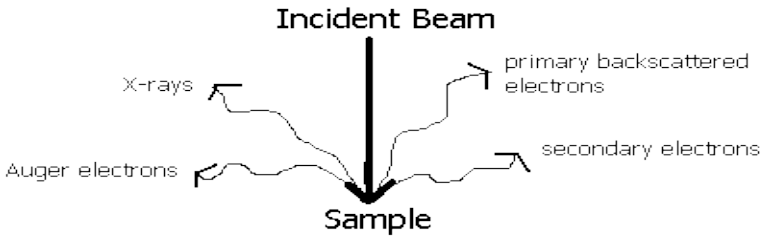

Fig. 4.4 X-Ray ejection from the sample

4.3.2 Preparation of Sample:

As the SEM utilizes vacuum conditions and uses electrons to form an image, special preparations must be done to the sample. All water must be removed from the samples because the water would vaporize in the vacuum. All metals are conductive and require no preparation before being used. All non-metals need to be made conductive by covering the sample with a thin layer of conductive material. This is done by using a device called a "sputter coater."

The sputter coater uses an electric field and argon gas. The sample is placed in a small chamber that is at a vacuum. Argon gas and an electric field cause an electron to be removed from the argon, making the atoms positively charged. The argon ions then become attracted to a negatively charged gold foil. The argon ions knock gold atoms from the surface of the gold foil. These gold atoms fall and settle onto the surface of the sample producing a thin gold coating.

4.4 Transmission Electron Microscopy:

Transmission electron microscopy (TEM) is a microscopy technique whereby a beam of electrons is transmitted through an ultra thin specimen, interacting with the specimen as it passes through. An image is formed from the interaction of the electrons transmitted through the specimen; the image is magnified and focused onto an imaging device, such as a fluorescent screen, on a layer of photographic film, or to be detected by a sensor such as a CCD camera.

4.4.1 Usage of Transmission Electron Microscopy

The transmission electron microscope is used to characterize the microstructure of materials with very high spatial resolution. Information about the morphology, crystal structure and defects, crystal phases and composition, and magnetic microstructure can be obtained by a combination of electron-optical imaging electron diffraction, and small probe capabilities.

Fig. 4.5 below shows a schematic outline of TEM.

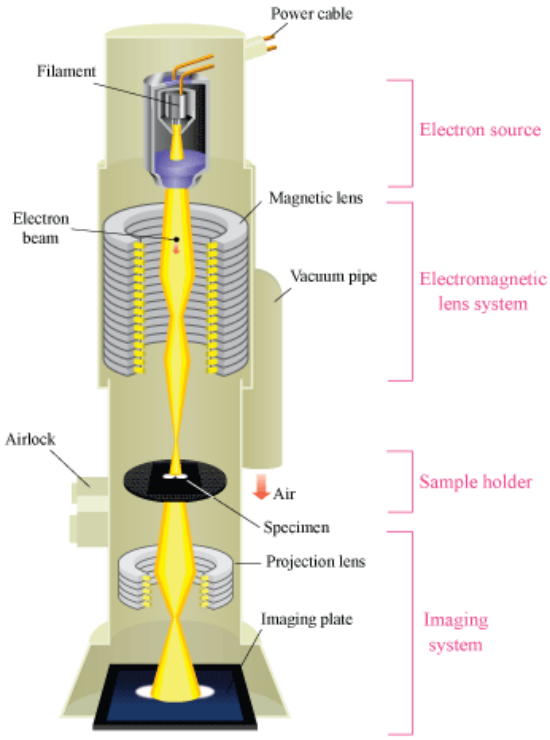

Figure 4.5 The schematic outline of a TEM.

A TEM contains four parts: electron source, electromagnetic lens system, sample holder, and imaging system.

1. Electron source

The electron source consists of a cathode and an anode. The cathode is a tungsten filament which emits electrons when being heated. A negative cap confines the electrons into a loosely focused beam (Fig. 3.6). The beam is then accelerated towards the specimen by the positive anode. Electrons at the rim of the beam will fall onto the anode while the others at the center will pass through the small hole of the anode. The electron source works like a cathode ray tube.

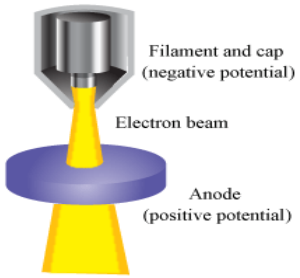

Fig. 4.6 Electron source of a TEM.

2. **Electromagnetic lens system**

After leaving the electron source, the electron beam is tightly focused using electromagnetic lens and metal apertures. The system only allows electrons within a small energy range to pass through, so the electrons in the electron beam will have a well-defined energy.

I. **Magnetic Lens**: Circular electro-magnets capable of generating a precise circular magnetic field. The field acts like an optical lens to focus the electrons.

II. **Aperture**: A thin disk with a small (2-100 micrometers) circular through-hole. It is used to restrict the electron beam and filter out unwanted electrons before hitting the specimen.

3.Sample holder

The sample holder is a platform equipped with a mechanical arm for holding the specimen and controlling its position.

4.Imaging system

The imaging system consists of another electromagnetic lens system and a screen. The electromagnetic lens system contains two lens systems, one for refocusing the electrons after they pass through the specimen, and the other for enlarging the image and projecting it onto the

screen. The screen has a phosphorescent plate which glows when being hit by electrons. Image forms in a way similar to photography.

4.4.2 Principal of Operation

The transmission electron microscope uses a high energy electron beam transmitted through a very thin sample to image and analyze the microstructure of materials with atomic scale resolution. The electrons are focused with electromagnetic lenses and the image is observed on a fluorescent screen, or recorded on film or digital camera. The electrons are accelerated at several hundred kV, giving wavelengths much smaller than that of light: 200kV electrons have a wavelength of 0.025Å. However, whereas the resolution of the optical microscope is limited by the wavelength of light, that of the electron microscope is limited by aberrations inherent in electromagnetic lenses, to about 1-2 Å.

Because even for very thin samples one is looking through many atoms, one does not usually see individual atoms. Rather the high resolution imaging mode of the microscope images the crystal lattice of a material as an interference pattern between the transmitted and diffracted beams. This allows one to observe planar and line defects, grain boundaries, interfaces, etc. with atomic scale resolution. The brightfield/darkfield imaging modes of the microscope, which operate at intermediate magnification, combined with electron diffraction, are also invaluable for giving information about the morphology, crystal phases, and defects in a material. Finally the microscope is equipped with a special imaging lens allowing for the observation of micromagnetic domain structures in a field-free environment.

The TEM is also capable of forming a focused electron probe, as small as 20 Å, which can be positioned on very fine features in the sample for micro diffraction information or analysis of x-rays for compositional information. The spatial resolution for this compositional analysis in TEM is much higher, on the order of the probe size, because the sample is so thin. Conversely the signal is much smaller and therefore less quantitative. The high brightness field-emission gun improves the sensitivity and resolution of x-ray compositional analysis over that available with more traditional thermionic sources

4.5 Viscometer

In general, either the fluid remains stationary and an object moves through it, or the object is stationary and the fluid moves past it. The drag caused by relative motion of the fluid and a surface is a measure of the viscosity. For the measurement of viscosity an instrument is used known as viscometer.

Viscometer Used And Specifications:

The viscosity of the nanofluids was measured using a Brookfield Viscometer (LV DV-IIICP) with a small sample adaptor. The adaptor consists of a cylindrical sample holder, a water jacket, and spindle. The viscometer drives the spindle immersed into the sample holder containing the test fluid sample. The viscometer provides a rotational speed that can be controlled to vary from 0.01 to 250 rpm yielding the shear rate (sec^{-1}) 3.84 N. It measures viscosity by measuring the viscous drag of the fluid against the spindle when it rotates. The spindle CPE-42 is used in these measurements as shown in fig. below. The sample holder can hold a small sample volume of 1 mL and the temperature of the test sample is monitored by a temperature sensor embedded into the water bath. Fig. 5.6 below shows the Brookfield Viscometer.

CHAPTER-5

METHODOLGY

5.1 Introduction

The main aim of this thesis is to prepare nanofluids with CuO nanoparticles and water and ethylene glycol as fluid for improving the heat transfer characteristics of the fluid. These analyses are performed by measuring viscosity at different temperatures for the different volume concentrations of nanofluids.

The other main aim of this thesis is to compare the results of water as base fluid with the ethylene glycol as base fluid for different concentrations.

5.2 Materials used for preparing Nanofluids

1. Nanoparticles- CuO (Average size- 40 nm)
2. Distilled water
3. Ethylene glycol

5.3 Preparation of Nanofluids

Copper oxide (CuO) nanoparticles were purchased from Reinste Nano Ventures lab, Noida. The size of nanoparticles is 40 nm as it was mentioned by the company. To confirm the material characterization, XRD is done at Panjab University, Chandigarh.XRD result is as shown below in fig 5.1.

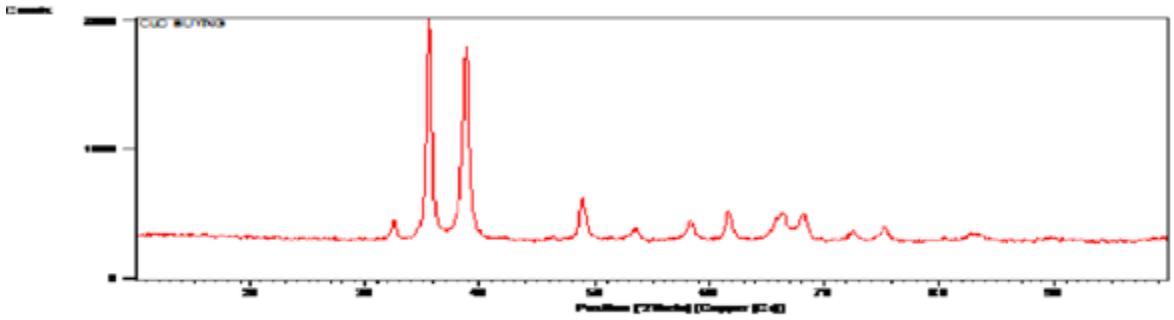

Fig 5.1 XRD result for CuO nanoparticle diameter 40 nm

Nanofluids are prepared by two step process. The resulting nanoparticles are then dispersed into the base fluid i.e. distilled water, ethylene glycol. Make the volume concentration of 0.005%,0.01%, 0.05% and .1 % by mixing 3.2 gm, 6.4 gm, 32gm and 64 gm of nanoparticles in 10 ml of distilled water and ethylene glycol. To make the nanoparticles more stable and remain more dispersed in water, ultra sonicator is used. Sonication had done for 3-4 hours before testing viscosity of the nanofluids. By this nanoparticles become more evenly dispersed in distilled water and ethylene glycol.

The CuO samples prepared are as shown in Fig. 5.2 is as shown below:

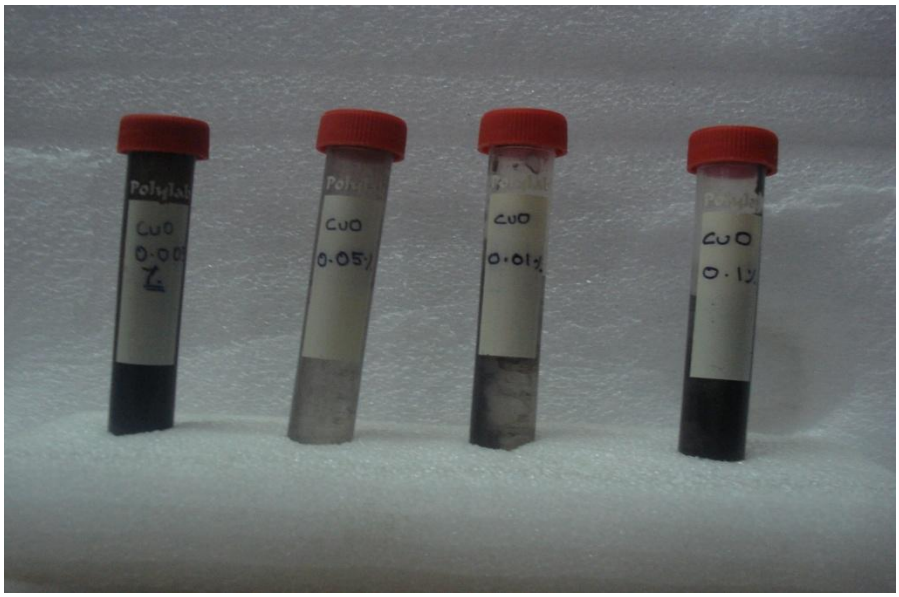

Fig. 5.2 CuO sample with different volumetric concentrations

5.4 Measurement of Viscosity

For the measurement of viscosity of nanofluids, Brookfield Viscometer (LV-DIII CP) is used as discussed in previous chapter. This is a new type of viscometer in which the amount of sample used is very less and is very accurate. It mainly consists up a cone, which is attached to the spindle of the viscometer and a plate which is usually the inner part of sample chamber in the instrument. For the temperature variation, a water bath is attached with the viscometer and its temperature range is from -10^{o}C to 100^{o}C. The arrangement is like in way that, water circulates from the outer portion of sample chamber and in this way the temperature of the sample chamber can be increased or decreased according to the requirement as shown in fig.5.3

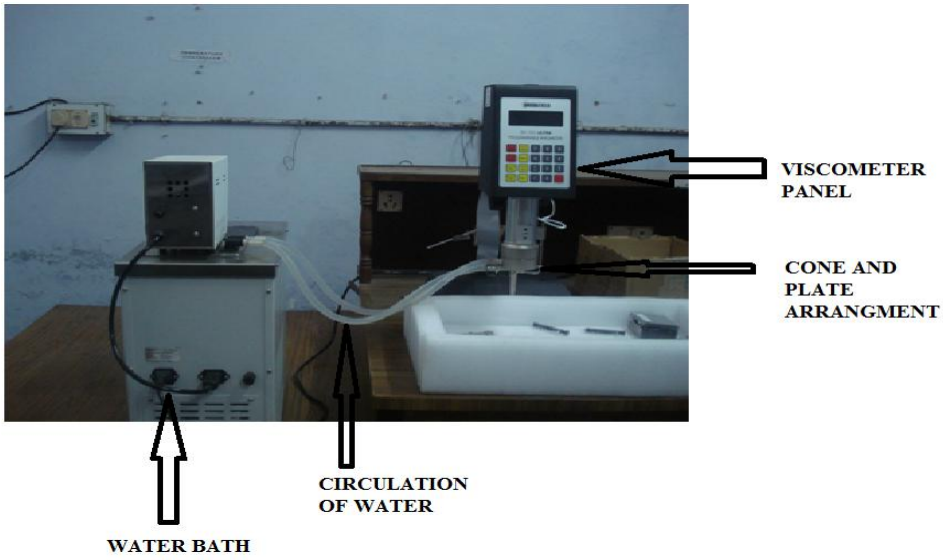

Fig. 5.3 Arrangement of water bath and viscometer

Before starting the viscometer, the main point is the gap setting. The gap in between the sample holder (plate) and the cone is 0.005 in. So this gap should be maintained properly and then maintain the temperature of sample chamber. After maintaining the gap and temperature, we can use the viscometer. Fig. 5.3 shows the gap indicator which indicates the gap in between the cone and sample chamber. Fig. 5.4 shows the cone which rotates inside the sample chamber.

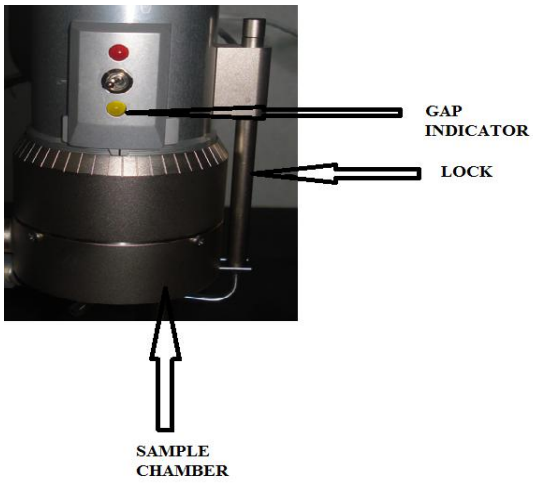

Fig. 5.4

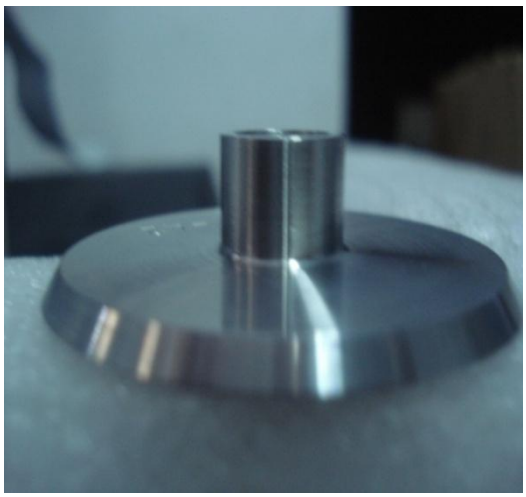

Fig. 5.5

CHAPTER 6

RESULTS AND DISCUSSION

Experiments are performed to measure the viscosity of water, ethylene glycol, CuO based nanofluid made from water and ethylene glycol and ethylene glycol mixed with water in 60:40 (by weight). A detailed report on the observed results is presented in this chapter.

6.1 Viscous Behavior of Water

The viscosity of distilled water was measured with in temperature range of 20^{o}C to 50^{o}C. The results of shear stress v/s shear rate and viscosity v/s water as shown below in the fig. 6.1 and 6.2.

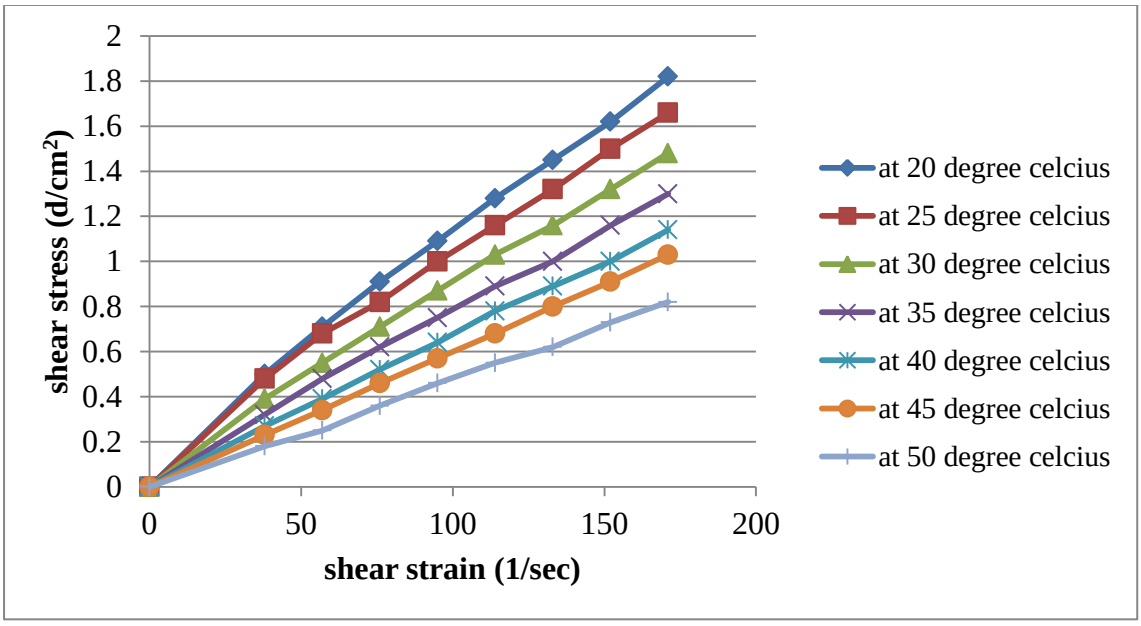

Fig. 6.1 Shear stress v/s shear rate at different temperatures

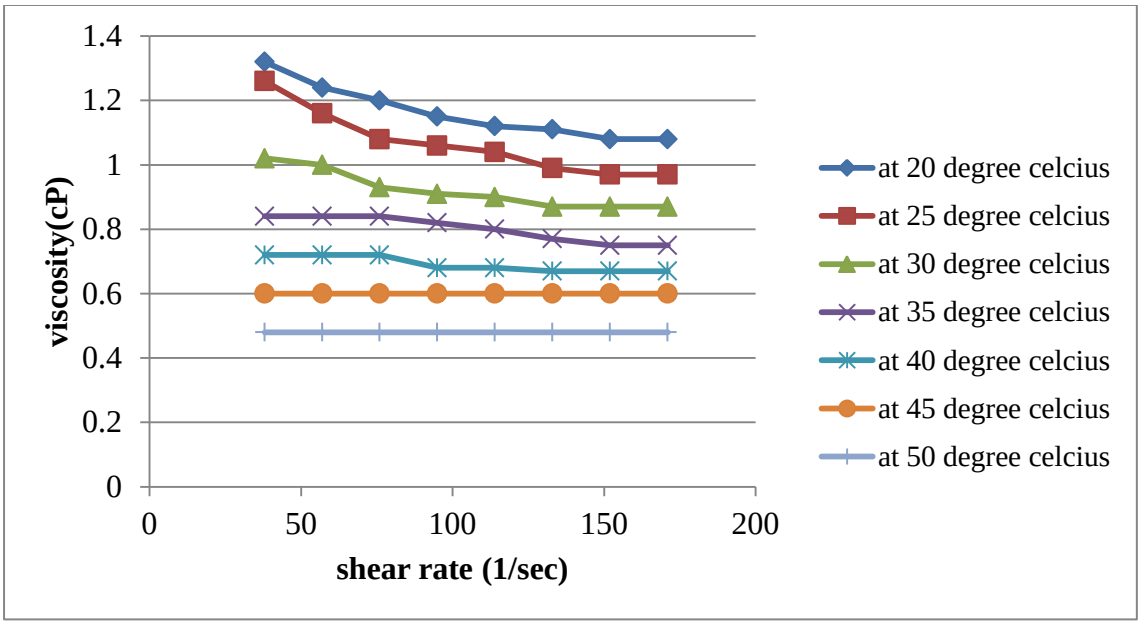

Fig.6.2 Viscosity v/s shear rate at different temperatures

The shear rate is same ($38sec^{-}1$ to $161sec^{-1}$) at each temperature but with the increase of temperature the shear stress is decreasing as shown in fig. 6.1. At low temperature water shows Non- Newtonian behaviour but as the temperature increases the Non- Newtonian behaviour of water changes into the Newtonian. Fig. 6.2 shows at $20^{o}C$ viscosity of water is 1.32cP and water is Non- Newtonian but as the temperature starts increases the viscosity starts decreasing and at $50^{o}C$ the viscosity is 0.48cP, completely Newtonian.

6.2 Viscous behavior of Ethylene Glycol (EG)

The results of shear stress v/s shear rate and viscosity v/s of water as shown below in the fig. 6.3 and 6.4.

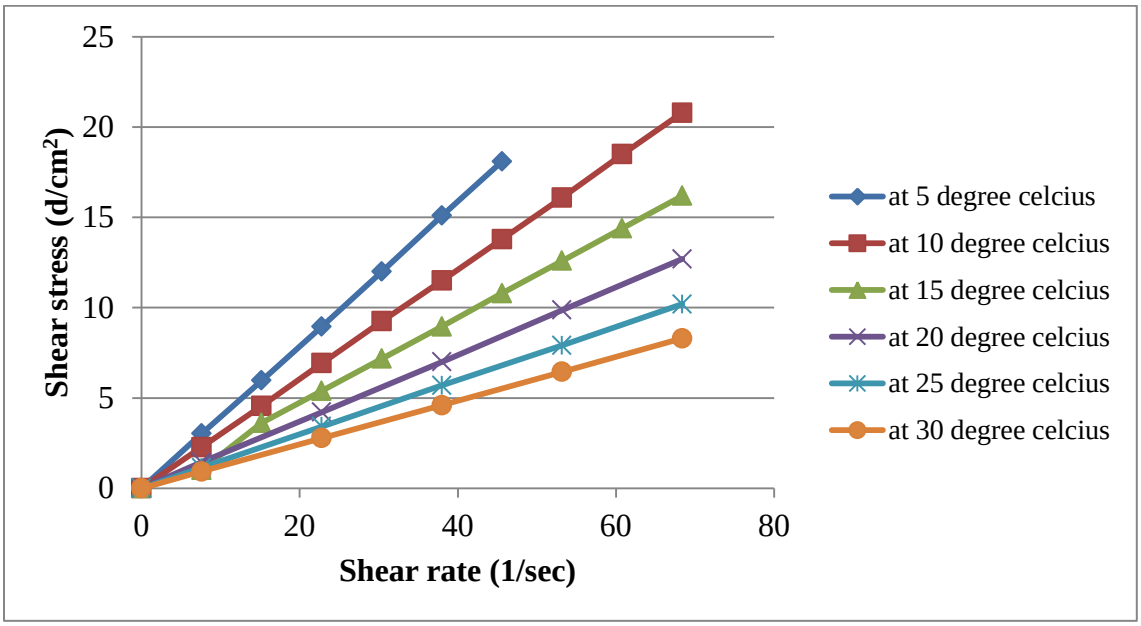

Fig. 6.3 Shear stress v/s shear rate at different temperatures

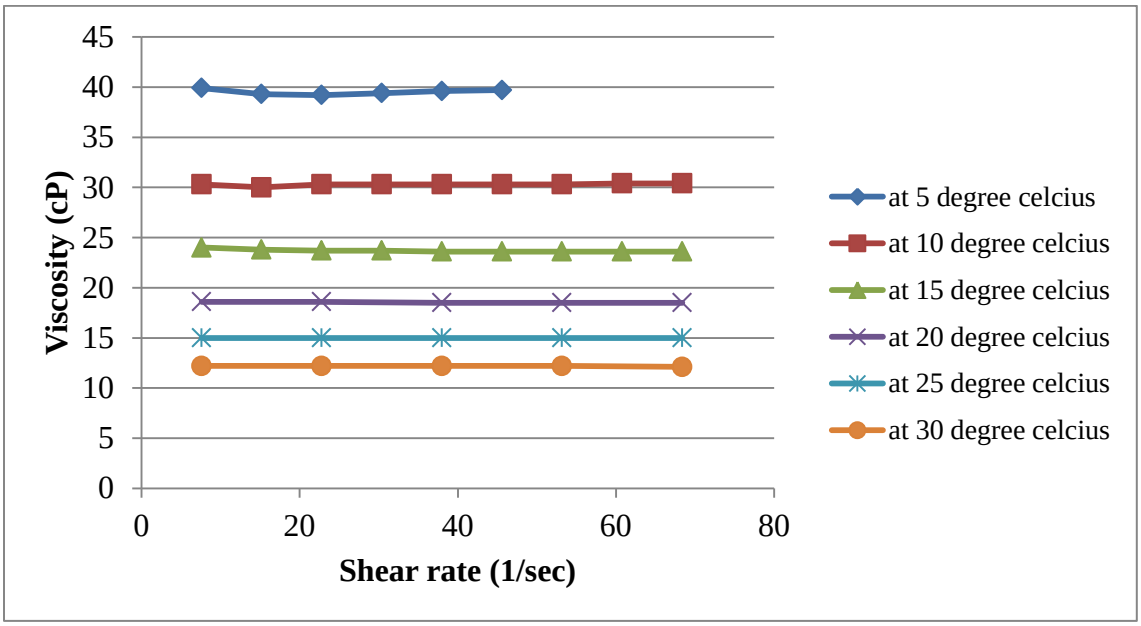

Fig. 6.4 Viscosity v/s shear rate at different temperatures

The shear rate(6.6 $sec^{-}1$ to 68.4 sec^{-1}) is same at each temperature but with the increase of temperature the shear stress is decreasing as shown in fig. 6.3. As Ethylene glycol is commonly used as antifreezing agent, so it is observed that even at 5°C it is showing almost Newtonian behaviour. Fig. 6.4 shows at 5°C the viscosity of ethylene glycol is 40cP and with the increase of temperature the viscosity starts decreasing, but the behaviour is Newtonian. Also it is clear that for temperature range 5°C- 30°C behaviour of EG is Newtonian.

6.3 Viscous behaviour of Ethylene Glycol (EG) with CuO nanoparticles

6.3.1 Ethylene glycol + CuO with 0.005% volumetric concentration

Fig. 6.5 and 6.6 shows the behavior of water when CuO was added in ethylene glycol with volumetric concentration of 0.005% at different temperatures.

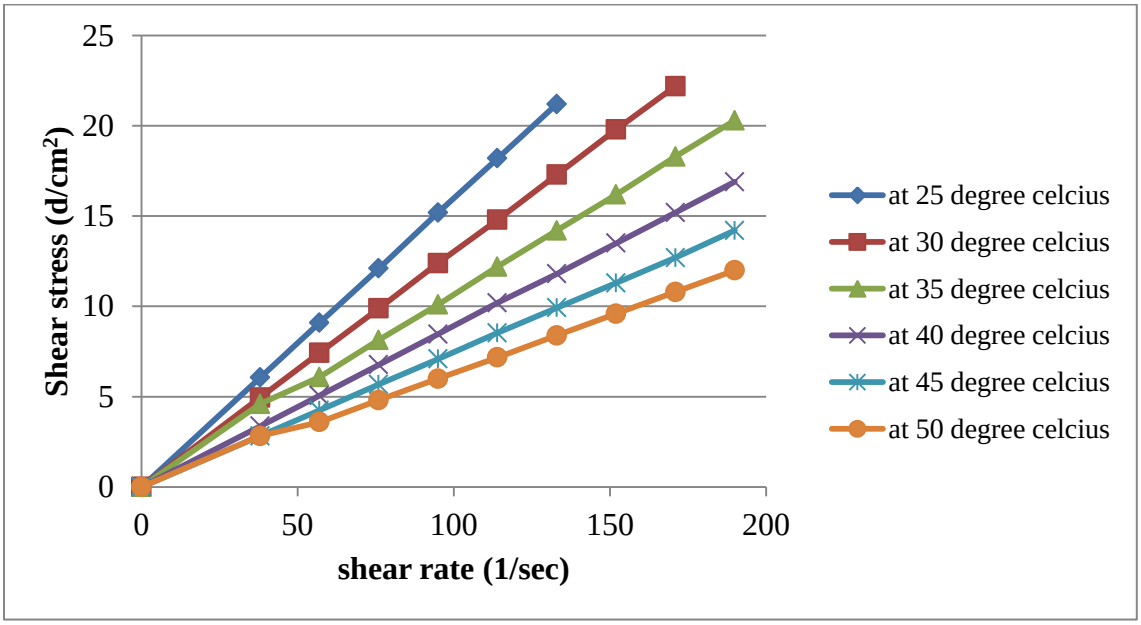

Fig. 6.5 Shear stress v/s shear rate for same volumetric concentration (0.005%) at different temperatures

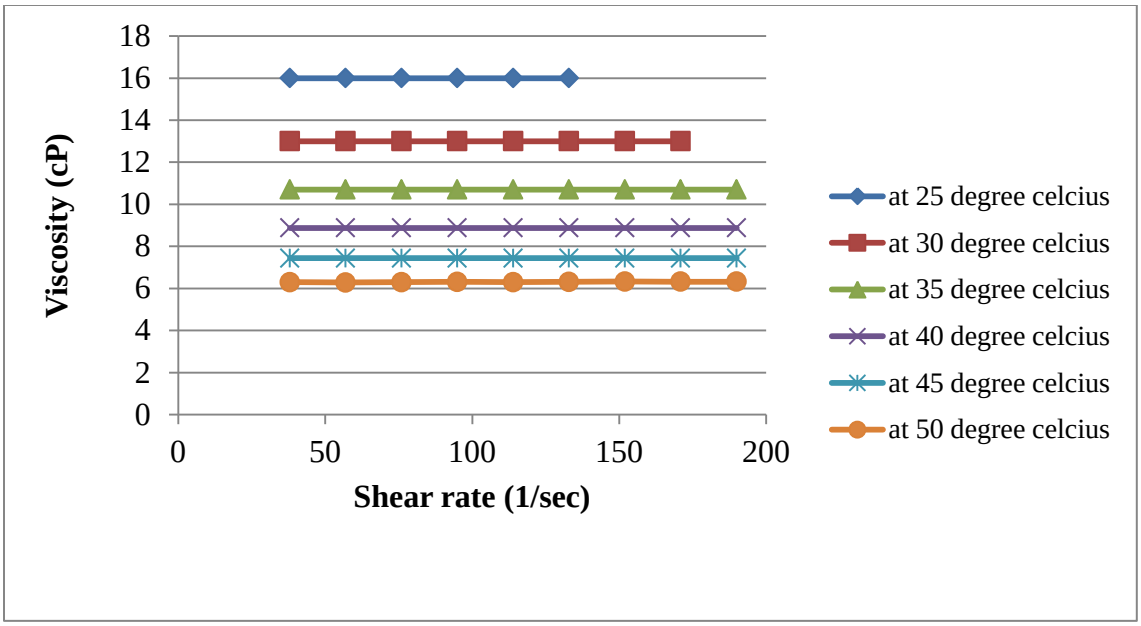

Fig. 6.6 Viscosity v/s shear rate for same volumetric concentration (0.005%) at different temperatures

6.3.2 Ethylene glycol + CuO with 0.01% volumetric concentration

Fig. 6.7 and 6.8 shows the behavior of water when CuO was added in ethylene glycol with volumetric concentration of 0.01% at different temperatures.

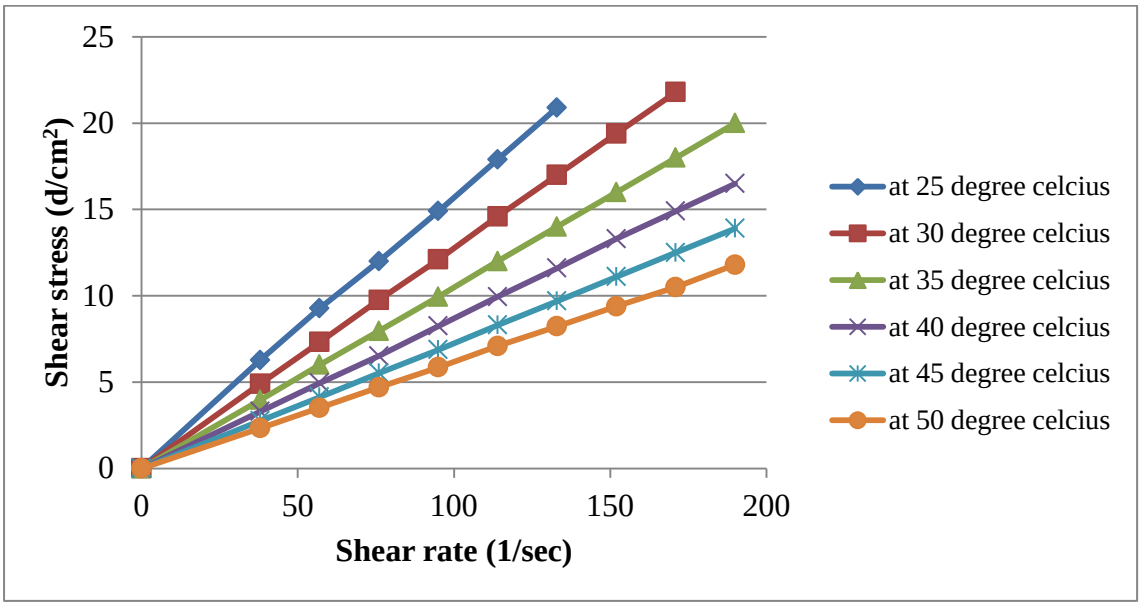

Fig. 6.7 Shear stress v/s shear rate for same volumetric concentration (0.01%) at different temperatures

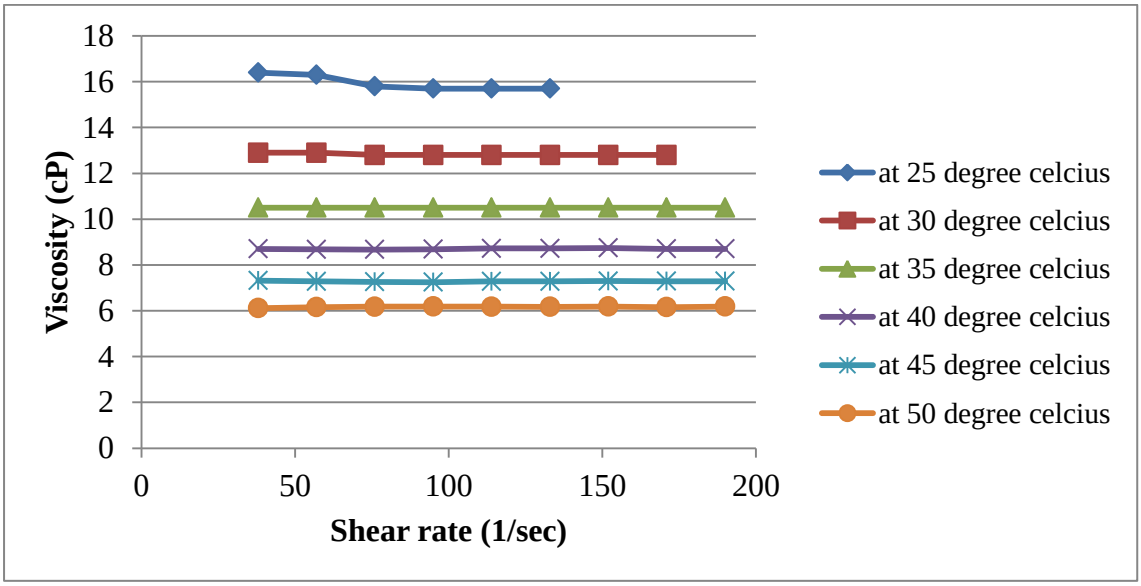

Fig. 6.8Viscosity v/s shear rate same volumetric concentration (0.01%) at different temperatures

6.3.3 Ethylene glycol + CuO with 0.05% volumetric concentration

Fig. 6.9 and 6.10 shows the behavior of water when CuO was added in ethylene glycol with volumetric concentration of 0.05% at different temperatures.

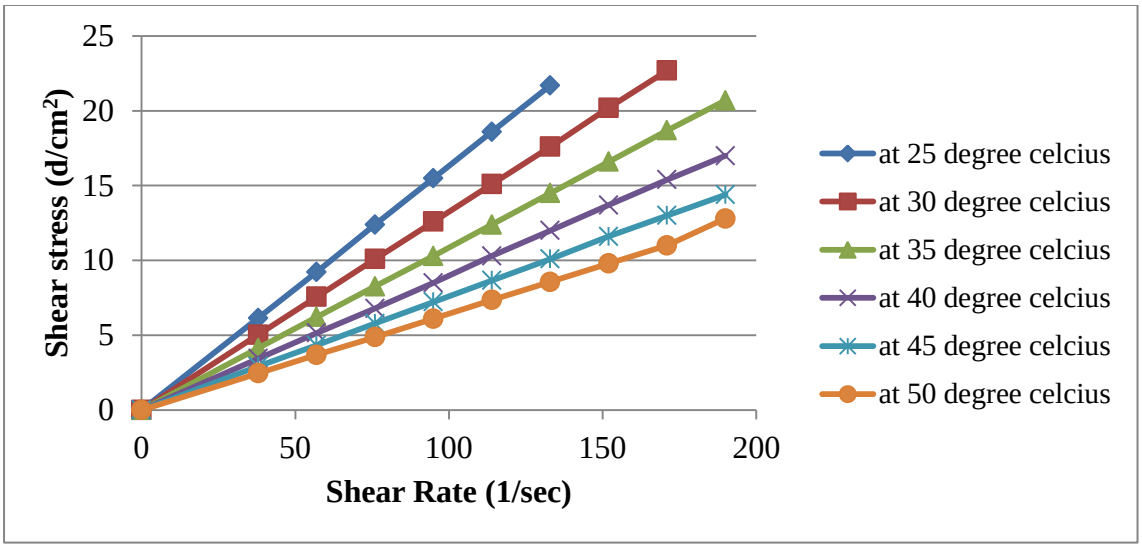

Fig. 6.9 Shear stress v/s shear rate for same volumetric concentration (0.05%) at different temperatures

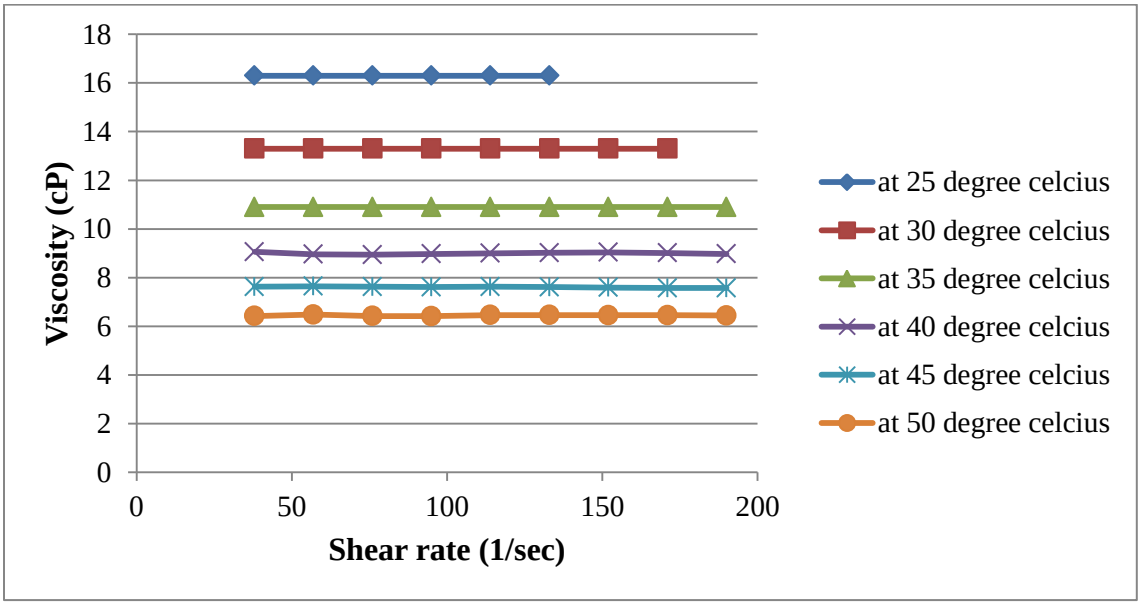

Fig. 6.10 Viscosity v/s shear rate same volumetric concentration (0.05%) at different temperatures

6.3.4 Ethylene glycol + CuO with 0.1% volumetric concentration

Fig. 6.11 and 6.12 shows the behavior of water when CuO was added in ethylene glycol with volumetric concentration of 0.1% at different temperatures.

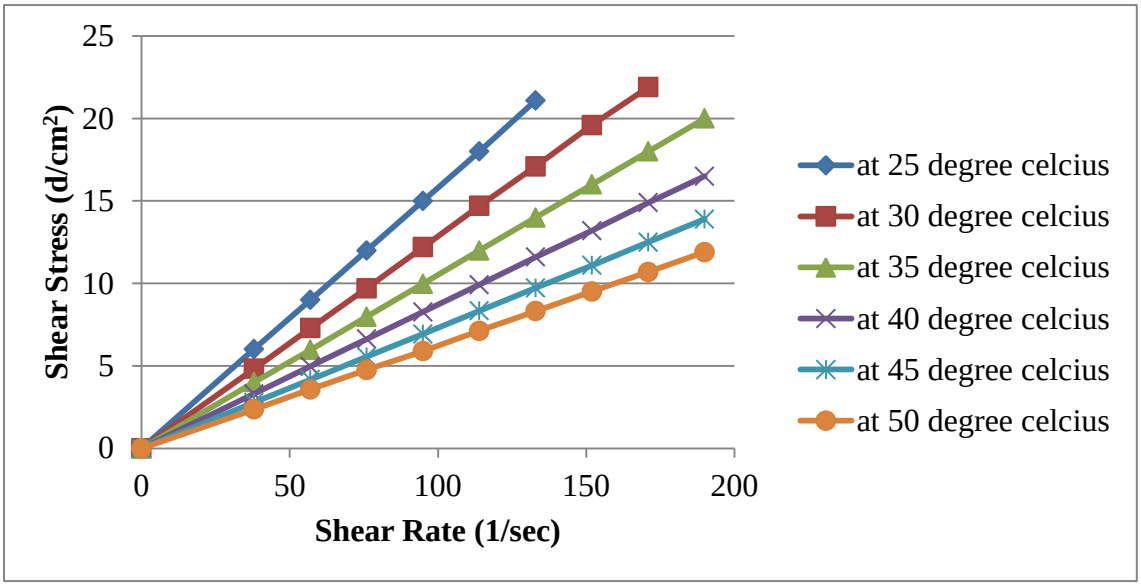

Fig. 6.11 Shear stress v/s shear rate for same volumetric concentration (0.05%) at different temperatures

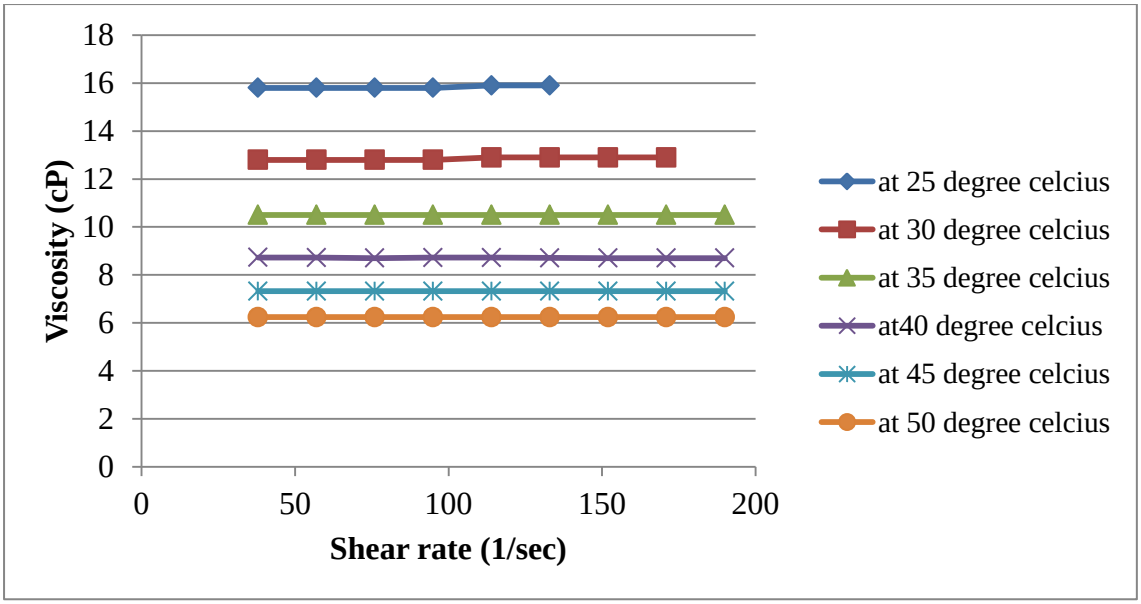

Fig. 6.12 Viscosity v/s shear rate same volumetric concentration (0.05%) at different temperatures

Ethylene glycol is commonly used in standard heating and cooling applications and its viscosity is 15 cP at room temperature. As viscosity is mainly responsible for energy consumption, so it becomes important to study the rheological behaviour of CuO-EG nanofluid under different conditions.

CuO nanoparticles by volumetric concentration of 0.005%, 0.05%, 0.01% and 0.1% are mixed with ethylene glycol. The results for shear stress and viscosity for above mentioned concentrations are as shown in fig. 6.5, 6.6, 6.7, 6.8, 6.9, 6.10, 6.11, 6.12 respectively, where CuO nanoparticles are added to ethylene glycol, the viscosity is found to increased to 16 cP for 0.005% at room temperature. Since it is very small concentration, but it shows 6.66 % increase in the viscosity, and for all measured concentrations behaviour remain Newtonian. It may be because of higher viscosity of EG which keeps the nanoparticles suspended in it.

6.4 Ethylene glycol, water (60:40)

Fig. 6.13 and 6.14 shows the behavior of ethylene glycol (60) : water (40) at different temperatures.

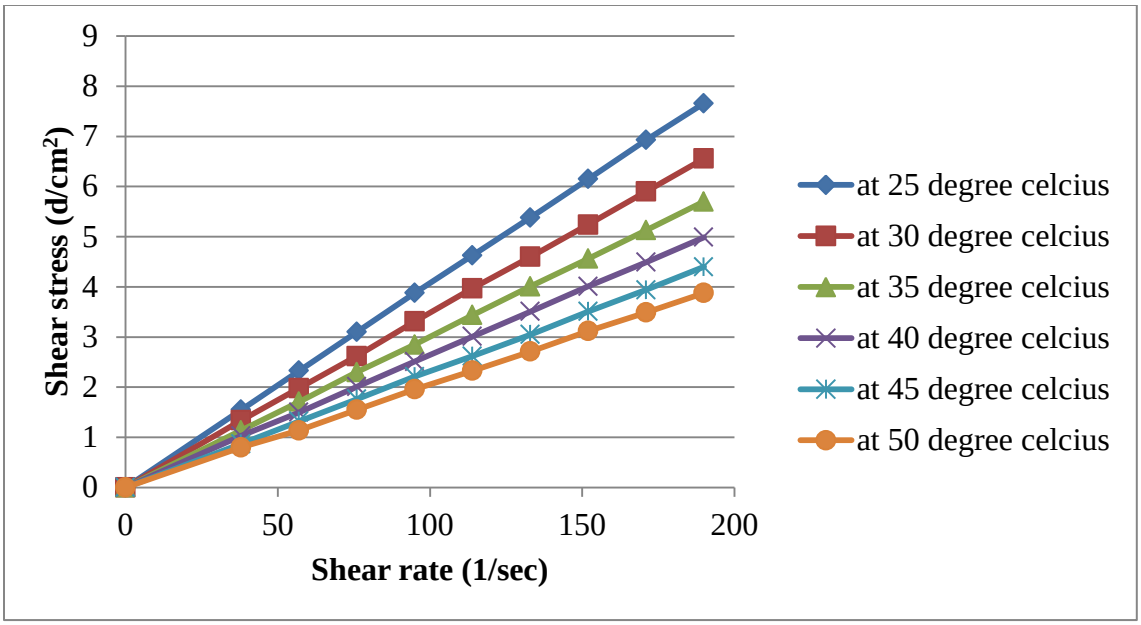

Fig. 6.13 Shear stress v/s shear rate at different temperatures

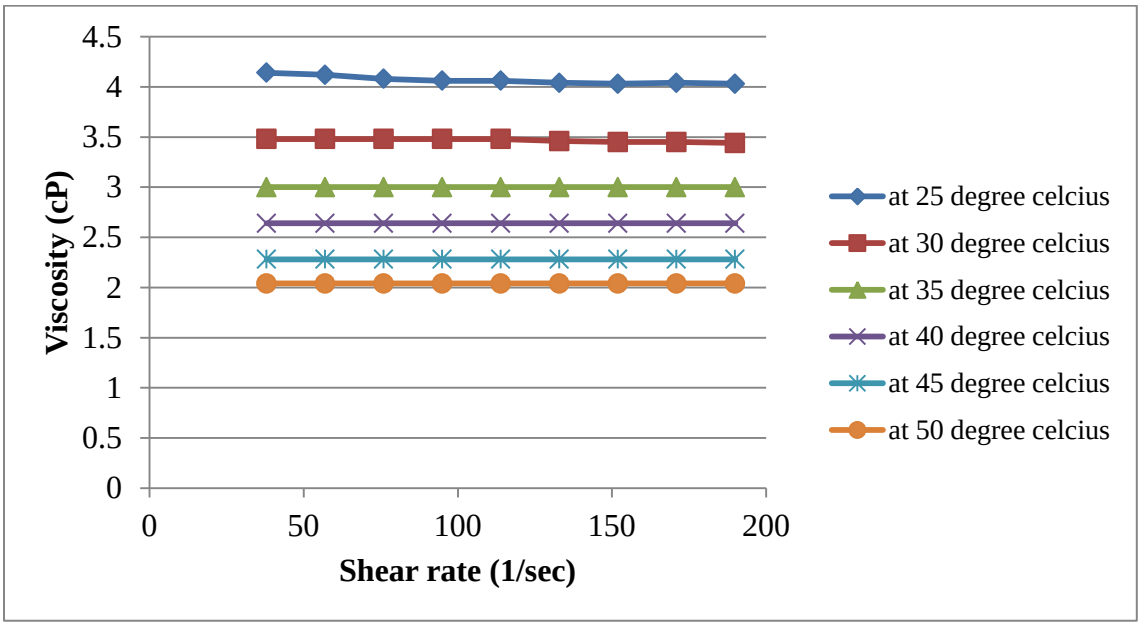

Fig. 6.14 Viscosity v/s shear rate at different temperatures

6.4.1 Ethylene glycol -water (60:40) with 0.005% volumetric concentration of CuO

Fig. 6.15 and 6.16 shows the behavior of ethylene glycol (60) : water (40) with CuO for 0.005% volumetric concentration .

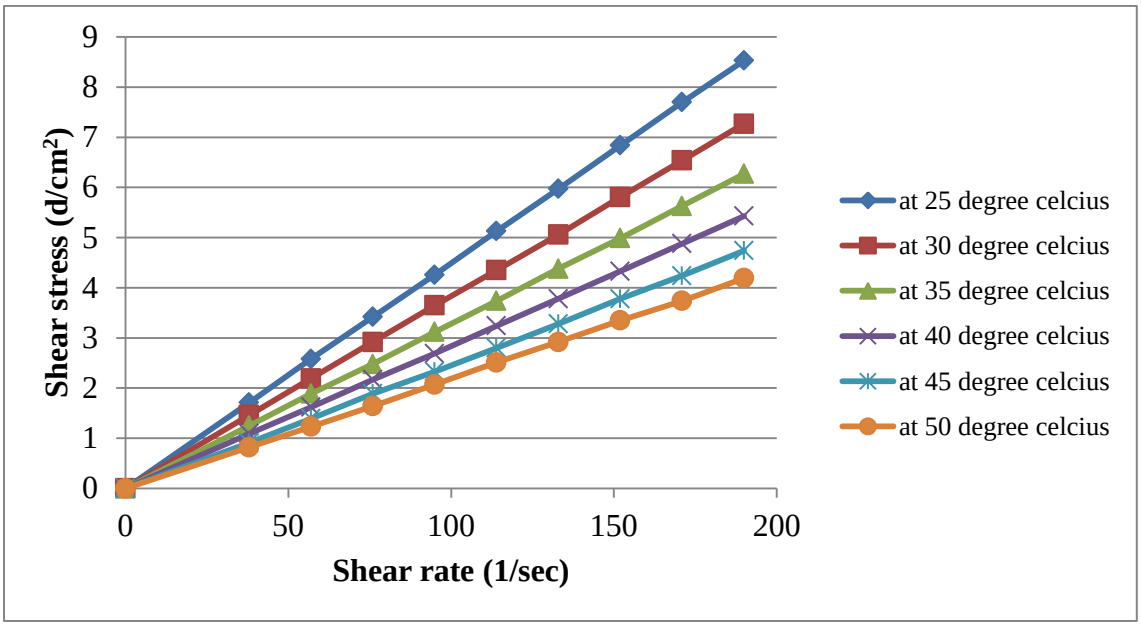

Fig. 6.15 Shear stress v/s shear rate for same volumetric concentration (0.005%) at different temperatures

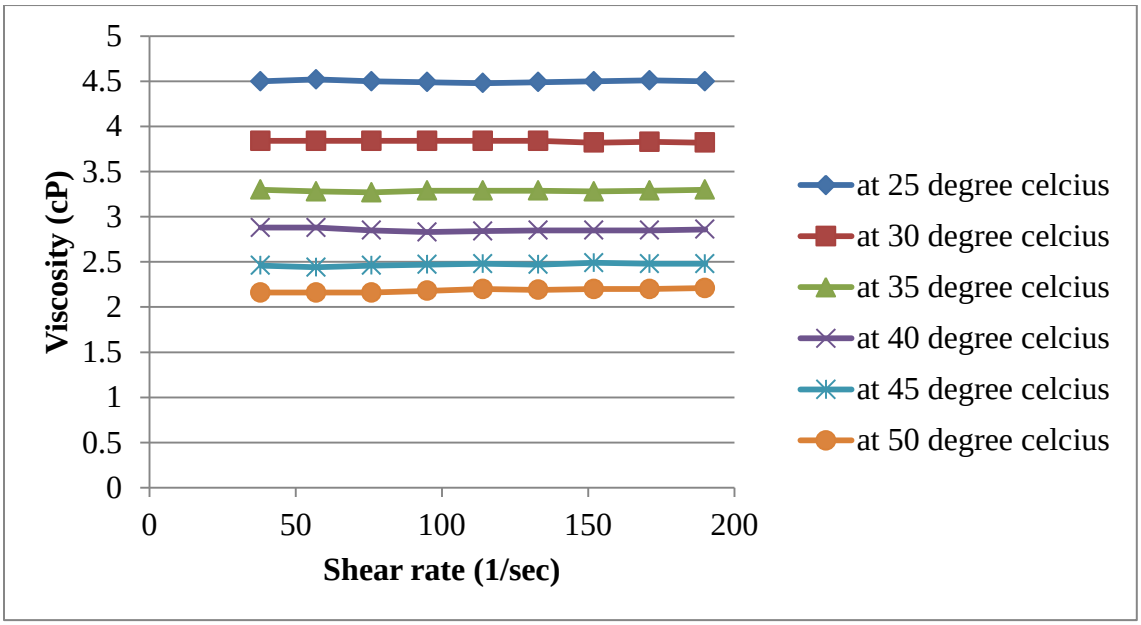

Fig. 6.16 Viscosity v/s shear rate for same volumetric concentration (0.005%) at different temperatures

6.4.2 Ethylene glycol (60): water (40) with CuO in 0.05% volumetric concentration

Fig. 6.17 and 6.18 shows the behavior of ethylene glycol (60) : water (40) with CuO in 0.05% volumetric concentration at same temperature.

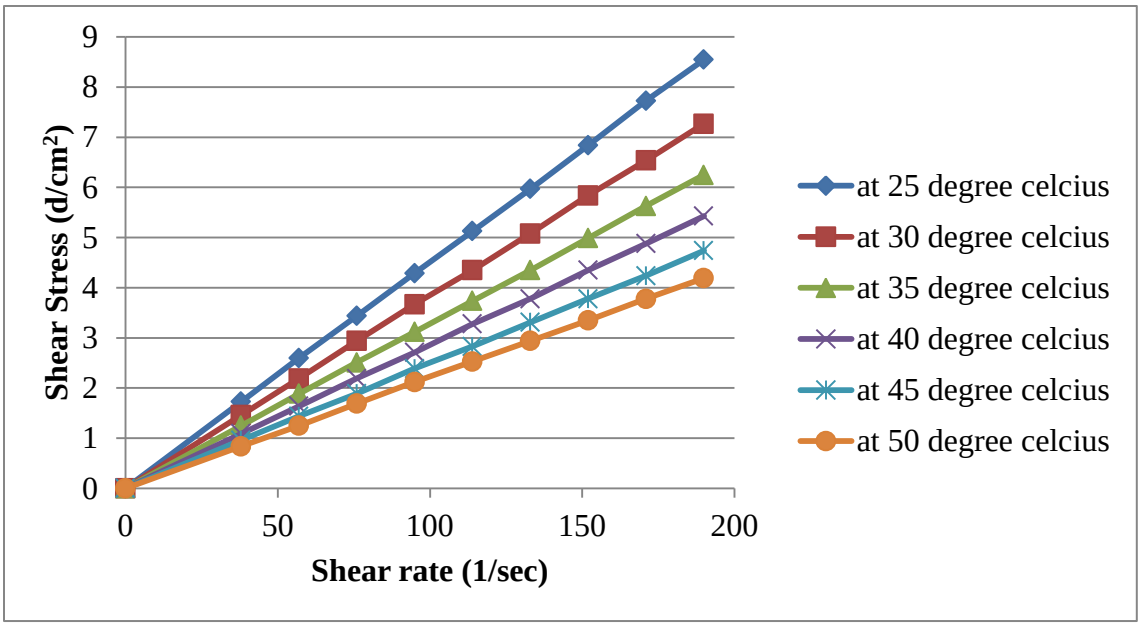

Fig. 6.17 Shear stress v/s shear rate for same volumetric concentration (0.05%) at different temperatures

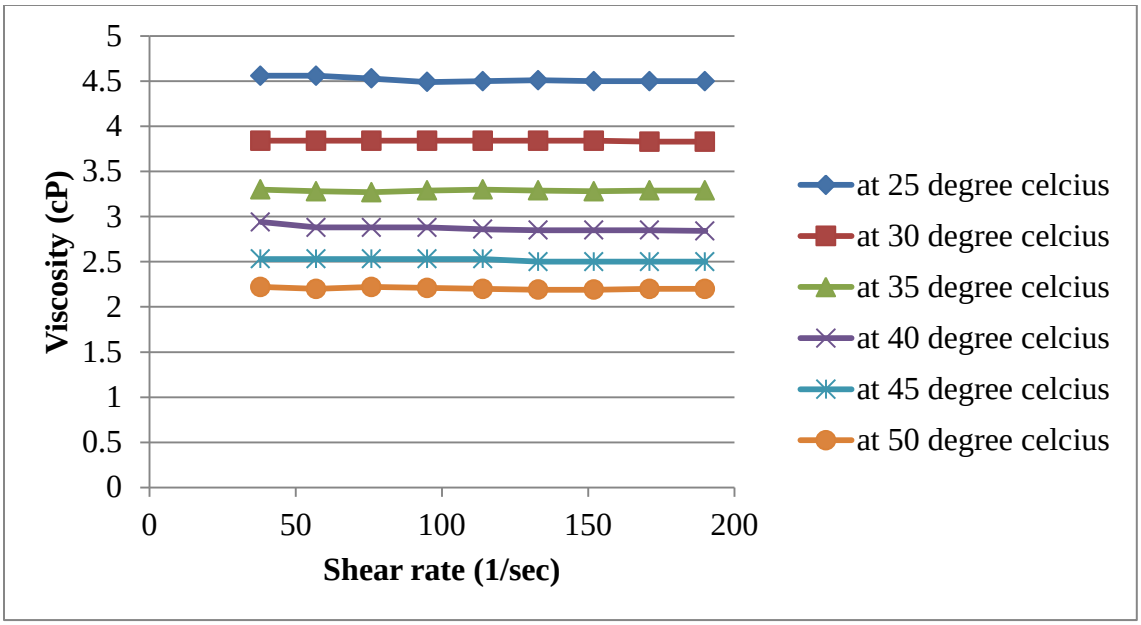

Fig. 6.18 Viscosity v/s shear rate for same volumetric concentration (0.05%) at different temperatures

Water is cheap and easily available coolant. So work is mainly going on water with nanoparticles to use it as nanofluid. But the major problem with water is settling down of the nanoparticles in it. On the other hand, ethylene glycol mixed with CuO shows good result with nanoparticles. So, we add ethylene glycol with water in 60:40 by weight to check the behavior of viscosity and it came 4.14 cP at room temperature. Then CuO nanoparticles were added to the solution(ethylene glycol+water) with 0.005% and 0.05%. With 0.005% volumetric concentration it shows 6.25% increase in viscosity and still the behavior remains Newtonian.

6.4 Viscosity and Temperature graphs for different volumetric concentrations

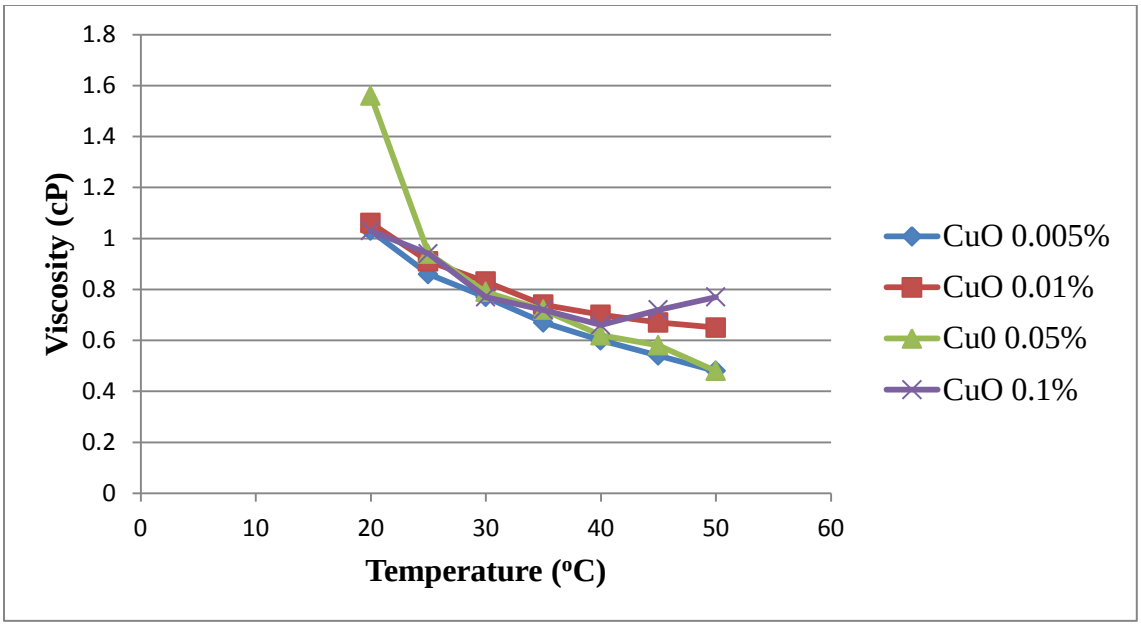

Fig. 6.19 Viscosity v/s temperature for CuO mixed with water at various concentrations

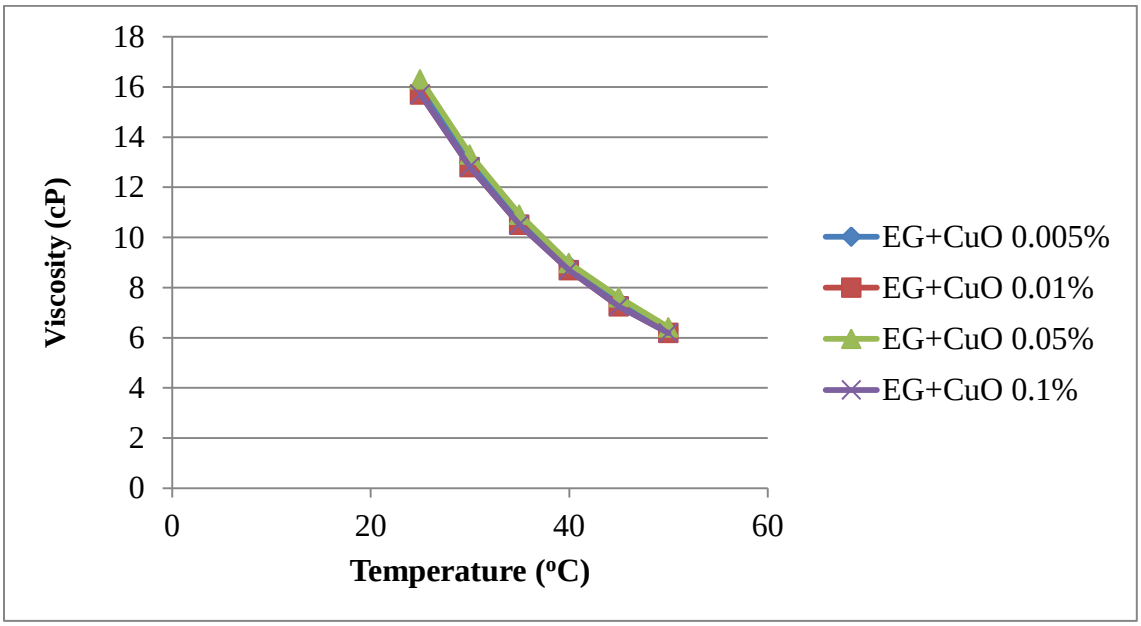

Fig.6.20 Viscosity v/s temperature for CuO mixed with ethylene glycol at various concentrations

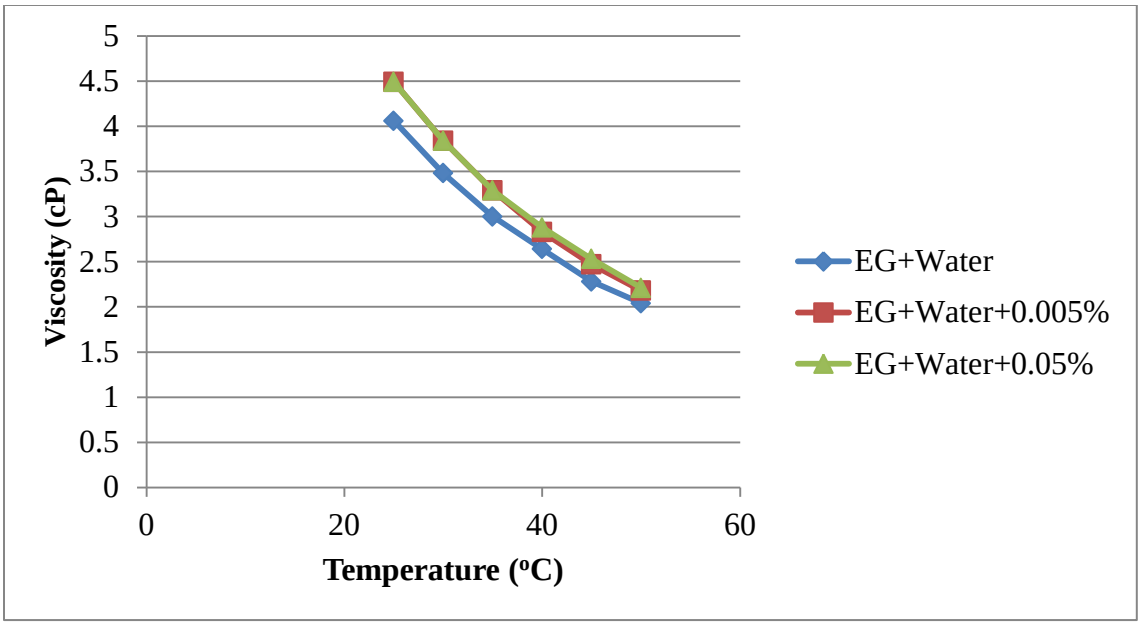

Fig.6.21 Viscosity v/s temperature for water mixed with ethylene glycol at various concentrations

Fig. 6.19 to 6.21 shows the relationship of fluids like water with CuO, Ethylene Glycol and ethylene glycol and water (60:40) with different volumetric concentrations at different temperatures. As the temperature increasing the viscosity of nanofluids is decreasing exponentially for every fluid. Fig. 6.20 is for the ethylene glycol and in this for all volumetric concentrations the viscosity is near to 16 cP. And it shows 6.67% increase in viscosity as compared to ethylene glycol without nanoparticle. Fig. 6.21 is for the EG and water (60:40) and in same way it's viscosity is decreasing with increase in temperature. Fig. 6.22 shows the behaviour of EG + CuO nanoparticles on viscosity with different volumetric concentrations. It shows that with the increase in temperature there is decrease in viscosity of nanofluid.

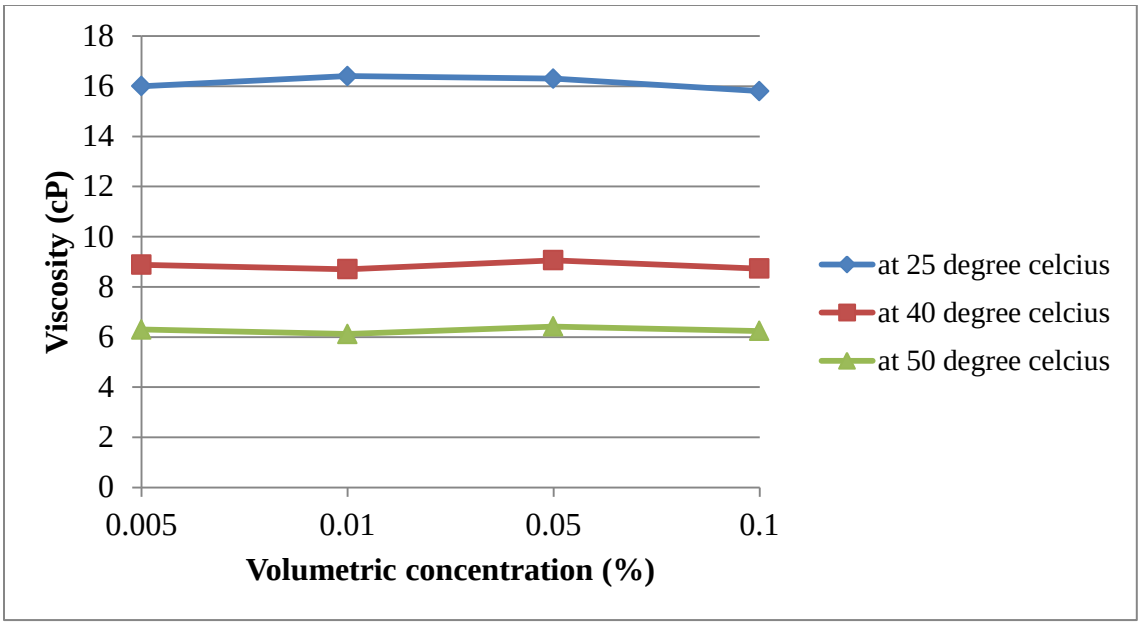

Fig. 6.22 Viscosity v/s volumetric concentration at different temperatures

CHAPTER 7

CONCLUSION

All results are concluded on the basis of the experiment performed for measuring the viscosity. This chapter summarizes the conclusion drawn in this report.

1. Nanofluids are dilute colloidal suspensions with nano-sized particles. It is prepared by dispersing the nanoparticles in base fluid and then put the samples in ultra sonicator to make the nanoparticles more suspended in the fluid and it also increases the stability of nanofluid.

2. CuO nanoparticles are added to ethylene glycol, the viscosity is found to increased to 16 cP for 0.005% at room temperature. Since it is very small concentration, but it shows 6.66 % increase in the viscosity.

3. Ethylene glycol with water in 60:40 by weight is used to study the behavior of viscosity of both as one fluid and its value found to be 4.14 cP at room temperature.

4. CuO nanoparticles are added to the solution (ethylene glycol+water) with 0.005% and 0.05%. With 0.005% volumetric concentration it shows 6.25% increase in viscosity and but behavior remains Newtonian.

5. The viscosity of nanofluids increases with increase in concentration of nanoparticles.

6. With the increases in temperature viscosity of copper oxide nanofluids decreases exponentially.

7. The relative viscosity of copper oxide nanofluids is dependent on volume percentage and decreases substantially with temperature for higher concentrations.

CHAPTER 8

APPLICATION AND FUTURE SCOPE

8.1 Introduction

Nanofluids are an exciting new category of more efficient heat transfer fluids that have the potential to greatly improve upon thermal management systems in a wide variety of applications, owing to their increased thermal conductivity and long term stability. Some of the applications of nanofluids are as follows:

They provide powerful cooling medium specially in the area of high density energy flux.

1. Crystal Silicon Mirror Cooling: One of the first applications of research in the field of nanofluids is for developing an advanced cooling technology to cool crystal silicon mirrors used in high intensity x-ray sources. Lee and Choi [80] carried out analysis to estimate the performance of microchannel heat exchangers with water, liquid nitrogen, and nanofluids as the working fluid.

2. Electronics Cooling: Chien et al. [81] were probably the first to show experimentally that the thermal performance of heat pipes can be enhanced by nearly a factor 2 when nanofluids are used. Water based nanofluids are used containing 16 nm gold nanoparticle as the working fluid in a disk-shaped miniature heat pipe (DMHP). Then, measured the thermal resistance of the DMHP with both nanofluids and deionized (DI) water. The results showed that thermal resistance of a DMHP reduced significantly (40%) when nanofluids were used instead of DI water.

3. Vehicle cooling: Nanoparticles can be dispersed not only in coolants and engine oils, but in transmission fluids, gear oils, and other fluids and lubricants. These may provide better overall thermal management and better lubrication. Tzeng et al. [82] were probably the first to apply nanofluid research in cooling a real-world automatic power transmission system. They dispersed CuO and Al_2O_3 nanoparticles into automatic transmission oil to investigate the optimum possible compositions of a nanofluid for higher heat transfer performance.

4. Transformer Cooling: The power generation industry is interested in transformer cooling application of nanofluids for reducing transformer size and weight. If the heat transfer capability

of existing transformers can be increased, many of the upgrades may not be necessary. Xuan and Li and Yu et al. [83,84] have demonstrated that the heat transfer properties of transformer oil can be improved by using nanoparticle additives.

5. Space and Nuclear Systems Cooling: You et al. [85] have discovered the unprecedented phenomenon that nanofluids can double or triple the CHF in pool boiling. Kim et al. [86] found that the high surface wet ability caused by nanoparticle deposition can explain this remarkable thermal property of nanofluid. The work is important in developing realistic predictive models of the CHF in nanofluids. The ability to greatly increase the CHF, the upper heat flux limit in nucleate boiling systems, is of paramount practical importance to ultra-high heat flux devices that use nucleate boiling, such as high power lasers and nuclear reactor components. Therefore nanofluids opened up exciting possibilities for raising chip power in electronic devices or simplifying cooling requirements for space applications.

8.2 Future Scope

Based upon the experimental investigation for CuO-H_2O nanofluid, it is proposed that the following areas may be considered for further investigations

1. The nanofluid can be used as a refrigerant in air conditioner and refrigerator.
2. Since by nanofluids the viscosity decreases, the pumping power required reduces. So it can be used for the cooling of engines and can be used in radiators.
3. It can be used as lubricating oil and engine oil.
4. Nanoparticles can be used for the purification of water

References

[1]. Choi SUS, Zhang ZG, Yu W, Lockwood FE, Grulke EA: Anomalous thermal conductivity enhancement in nano tube suspensions. Appl Phys Lett 2001, 69:2252.

[2]. Xie H, Fujii M, Zhang X: Effect of interfacial nanolayer on the effective thermal conductivity of nanoparticle-fluid mixture. Int J Heat Mass Transfer 2005, 48:2926.

[3]. Wang XQ, Mujumdar AS: Heat transfer characteristics of nanofluids: a review. Int J Therm Sci 2006, 46:1.

[4]. Masoumi N, Sohrabi N, Behzadmehr A: A new model for calculating the effective viscosity of nanofluids. J Phys D Appl Phys 2009, 42:055501.

[5]. Nguyen CT, Desgranges F, Roy G, Galanis N, Mare T, Boucher S, Angue Mintsa H: Temperature and particle-size dependent viscosity data for water-based nanofluids - Hysteresis phenomenon. Int J Heat Fluid Flow 2006, 28:1492.

[6]. Einstein A: A new determination of the molecular dimensions. Ann Phys 1906, 19:289.

[7]. Brinkman HC: The viscosity of concentrated suspensions and solution. J Chem Phys 1952, 20:561.

[8]. Frankel NA, Acrivos A: On the viscosity of a concentrated suspension of solid spheres. Chem Eng Sci 1966, 22:846.

[9]. Lundgren TS: Slow flow through stationary random beds and suspensions of spheres. J Fluid Mech 1962, 51:263.

[10]. Batchelor GK: The effect of Brownian motion on the bulk stress in a suspension of spherical particles. J Fluid Mech 1966, 83:96.

[11]. Graham AL: On the viscosity of suspension of solid spheres. Appl Sci Res 1981, 36:265.

[12]. Das K Sarit, Choi U.S Stephen, Wenhua Yu and Pradeep T. (2006). Nanofluids: Science and Technology. John Wiley & Sons, Inc. New Jersey. pp. 1-2.

[13] A. Einstein, Eine neue bestimmung der molekuldimensionen, Ann. Phys., Leipzig 19 (1906) 289–306.
[14] H.C. Brinkman, The viscosity of concentrated suspensions and solutions, J.Chem. Phys. 20 (1952) 571.
[15] G. Batchelor, The effect of Brownian motion on the bulk stress in a suspension of spherical particles, J. Fluid Mech. 83 (1977) 97–117.
[16] T. Lundgren, Slow flow through stationary random beds and suspensions of spheres, J. Fluid Mech. 51 (1972) 273–299.
[17] A.L. Graham, On the viscosity of suspensions of solid spheres, Appl. Sci. Res. 37 (1981) 275–286.
[18] R.A. Simha, Treatment of the viscosity of concentrated suspensions, J. Appl. Phys. 23 (1952) 1020–1024.
[19] M. Mooney, The viscosity of a concentrated suspension of spherical particles, J. Colloid Sci. 6 (1951) 162–170.
[20] V.H. Eilers, Die viskocitat von emulsionen hochviskoser stoffe als funktion der konzentration, Kolloid-Zeitschrift 97 (1941) 313–321.
[21] N. Saito, Concentration dependence of the viscosity of high polymer solutions, J. Phys. Soc. Jpn. 5 (1950) 4–8.
[22] N.A. Frankel, A. Acrivos, On the viscosity of a concentrate suspension of solid spheres, Chem. Eng. Sci. 22 (1967) 847–853.
[23]. Kurosaki Y and Murasaki T (1986). Study on Heat Transfer Mechanism of a Gas Solid

Suspension Impinging Jet (Effect of Particle Sizes and Thermal Properties). Proceedings of

the Eighth International Heat Transfer Conference, Volume 5, Hemisphere, Washington, D.C. pp. 2586.2592.

[24]. Murray D.B (1994). Local Enhancement of Heat Transfer in a Particulate Cross Flow1.

International Journal of Multiphase Flow, Volume 20. Issue 3. pp. 493.504.

[25]. Avila R, and Cervantes J (1995). Analysis of the Heat Transfer Coefficient in a Turbulent Particle Pipe Flow. International Journal of Heat and Mass Transfer, Volume 38. Issue 11. pp. 1923.1932.

[26]. Ouyang S, Li X.-G, Davies G, and Potter O. E (1996). Heat Transfer between a Vertical Tube Bundle and Fine Particles in a CFB Downcomer with and without Circulation of Solids.Chemical Engineering and Processing, Volume 35. Issue 1. pp. 21.26.

[27]. Artus G R C (1996). Measurements of the Novel Thermal Conduction of a Porphoritic Heat Sink Paste. IEEE Transactions on Components, Packaging, and Manufacturing - Part B, Volume 19. Issue 3. pp. 601.604.

[28]. Eastman J A, Choi U. S, Li S, Thompson L J, and Lee S (1996). Enhanced Thermal Conductivity through the Development of Nanofluids. Materials Research Society Symposium Proceedings, Volume 456. Materials Research Society, Pittsburgh, PA. pp. 3.11.

[20]. Li H C and Peterson G P (2006). Appl. Phys. Letter, Volume 99. pp. 1.8.

[29]. Choi U S, Zhang Z G and Keblinski P (2004). Encyclopedia of Nanoscience and Nanotechnology. American Scientific Publishers, Volume 6. pp. 656.663.

[30]. Nguyen N T, Ting T H, Yap Y F, Wong T N Chai, J C K, Ong W L, Zhou J L, Tan S H and Yobas L (2006). Appl. Phys. Letter, Volume 91. pp. 1.3.

[32]. A. Einstein, Eine neue bestimmung der molekuldimensionen, Ann. Phys.,Leipzig 19 (1906) 289–306.

[32] H. Akoh, Y. Tsukasaki, S. Yatsuya, A. Tasaki, Magnetic properties of ferromagnetic ultrafine particles prepared by vacuum evaporation on running oil substrate, Journal of Crystal Growth 45 (1968) 495–500.

[33] M. Wagener, B.S. Murty, B. Gunther, Preparation of metal nanosuspensions by high-pressure DC-sputtering on running liquids, in: S. Komarnenl, J.C. Parker, H.J. Wollenberger (Eds.), Nanocrystalline and Nanocomposite Materials II, vol. 456, Materials Research Society, Pittsburgh, PA, 1996, pp. 149–154.

[34] J.A. Eastman, U.S. Choi, S. Li, L.J. Thompson, S. Lee, Enhanced thermal conductivity through the development of nanofluids, Materials Research Society Symposium – Proceedings, vol. 456, Materials Research Society, Pittsburgh, PA, USA, Boston, MA, USA, 1996, pp. 3–11.

[35] C.-H. Lo, T.-T. Tsung, L.-C. Chen, Shape-controlled synthesis of Cubased nanofluid using submerged arc nanoparticle synthesis system (SANSS), Journal of Crystal Growth 266 (1–4) (2005) 636–642.

[36] C.-H. Lo, T.-T. Tsung, L.-C. Chen, Ni nano-magnetic fluid prepared by submerged arc nano synthesis system (sanss), JSME International Journal, Series B: Fluids and Thermal Engineering 48 (4) (2006) 650–655.

[36]. Granqvist C.G and Buhrman R.A (1966). Ultra-fine metal particles. J.Appl. Physics, Volume 46. pp. 2200.

[37]. Romano J.M, Parker J.C, and Ford Q.B (1996). Application opportunities for nanoparticles made from condensation of physical vapors. Adv. Powder Methal. Partic. Mater, Volume 2. pp.12-13.

[38]. Robert J. H (1989). Foundations of Colloid Science. Oxford University Press, Volume 2. pp.684.

[39]. Lurio L. B, Lumma D, Borthwick M. A, Falus P, Mochrie S. G. J, Pelletier J. F, and Sutton M (2000). Creating Coherent X-rays and Putting them to Use: X-Ray Photon Correlation Spectroscopy at Beamline 8-ID at the Advanced Photon Source. Synchrotron Radiat News, Volume 13. pp. 28-38.

[40]. Praveen KN, Devdatta PK, Misra D, Das DK: “Viscosity of copper oxide nanoparticles dispersed in ethylene glycol and water mixture”. Exp ThermFluid Sci 2007, 32:397-402.

[41]. Nguyen CT, Desgranges F, Roy G, Galanis N, Mare T, Boucher S, Angue Mintsa H: “Temperature and particle-size dependent viscosity data for water-based nanofluids - Hysteresis phenomenon”. Int J Heat Fluid Flow 2007, 28:1492.

[42] D.P. Kulkarni, D.K. Das, S.L. Patil: “Effect of temperature on rheological properties of copper oxide nanoparticles dispersed in propylene glycol and water mixture”, J. Nanosci Nanotechnol. 7 (2007) 2318–2322.

[43] P.K. Namburu, D.P. Kulkarni, A. Dandek ar and D.K. Das "Experimental investigation of viscosity and specific heat of silicon dioxide nanofluids" Micro & Nano Letters, Vol. 2, No. 3, September 2006.

[44]. Prasher Ravi, Song David, and Wang Jinlin (2006). Measurement of nanofluid viscosity and its implications for thermal applications. Applied Phys. Lett., Volume 89. Issue 13. pp. 133108 - 133108-3.

[45]. Zhou Le.Ping, Wang Bu.Xuan, Peng Xiao.Feng, Xiao Ze.Du, and Yang Yong.Ping (2009). On the Specific Heat Capacity of CuO Nanofluid. Advances in Mechanical Engineering, Volume 2010. Article ID 162085. pp. 1-4.

[46]. Sheng-Qi Zhoua and Rui Ni (2008). Measurement of the specific heat capacity of water-based Al_2O_3 nanofluid. Applied Physics Letters, Volume 92. Issue 09. pp. 3123.

[41]. Prasher Ravi, Song David, and Wang Jinlin (2006). Measurement of nanofluid viscosity and its implications for thermal applications. Applied Phys. Lett., Volume 89. Issue 13. pp. 133108 - 133108-3.

[42]. Zhou Le.Ping, Wang Bu.Xuan, Peng Xiao.Feng, Xiao Ze.Du, and Yang Yong.Ping (2009). On the Specific Heat Capacity of CuO Nanofluid. Advances in Mechanical Engineering, Volume 2010. Article ID 162085. pp. 1-4.

[43]. Sheng-Qi Zhoua and Rui Ni (2008). Measurement of the specific heat capacity of water-based Al_2O_3 nanofluid. Applied Physics Letters, Volume 92. Issue 09. pp. 3123.

[44]. Praveen KN, Devdatta PK, Misra D, Das DK: Viscosity of copper oxide nanoparticles dispersed in ethylene glycol and water mixture. Exp ThermFluid Sci 2007, 32:397-402.

[45]. Nguyen CT, Desgranges F, Roy G, Galanis N, Mare' T, Boucher S, Angue Mintsa H: Viscosity data for Al2O3-water nanofluid–hysteresis: is heat transfer enhancement using nanofluids reliable? Int J Therm Sci 2008, 47:103-111.

[46]. Chen H, Ding Y, Lapkin A: Rheological behaviour of nanofluids containing tube/rod-like nanoparticles. Powder Technol 2009, 194:132-141.

[47]. Phuoc TX, Massoudi M: Experimental observations of the effects of shear rates and particle concentration on the viscosity of Fe2O3-deionized water nanofluids. Int J Therm Sci 2009, 48:1294-1301.

[48]. Garg P, Alvarado JL, Marsh C, Carlson TA, Kessler DA, Annamalai K: An experimental study on the effect of ultrasonication on viscosity and heat transfer performance of multi-wall carbon nanotube-based aqueous nanofluids. Int J Heat Mass Transf 2009, 52:5090-5101.

[49]. Murshed SMS, Leong KC, Yang C: Investigations of thermal conductivity and viscosity of nanofluids. Int J Therm Sci 2008, 47:560-568.

[50]. Chena H, Witharana S, Jina Y, Kimd C, Ding Y: Predicting thermal conductivity of liquid suspensions of nanoparticles (nanofluids) based on rheology. Particuology 2009, 7:151-157.

[51]. Lee JH, Hwang KS, Jang SP, Lee BH, Kim JH, Choi SUS, Choi CJ: Effective viscosities and thermal conductivities of aqueous nanofluids containing low volume concentrations of Al2O3 nanoparticles. Int J Heat Mass Transfer 2008, 51:2651-2656.

[52]. Nguyen CT, Desgranges F, Roy G, Galanis N, Mare T, Boucher S, Angue Mintsa H: Temperature and particle-size dependent viscosity data for water-based nanofluids - Hysteresis phenomenon. Int J Heat Fluid Flow 2007, 28:1492-1506.

[53].Duangthongsuk W, Wongwises S: Measurement of temperature dependent thermal conductivity and viscosity of TiO2-water nanofluids. Exp Therm Fluid Sci 2009, 33:706-714.

[54] Bell A T 2003 *Science* **299** 1668

[55] Bond G C and Thompson D T 1999 *Catal. Rev. Sci. Eng.* **41** 319

[56] Li P, Miser D E, Rabiei S, Yadav R T and Hajaligol M R 2003 *Appl. Catal.* B **43** 151

[57] Stoimenov P K, Zaikovski V and Klabunde K J 2003 *J. Am. Chem. Soc.* **125** 12906

[58] Joh´anek V, Laurin M, Grant A W, Kasemo B, Henry C R and Libuda J 2004 *Science* **304** 1639

[59] Schl¨ogl R and Abd Hamid S B 2004 *Angew. Chem. Int. Edn* **43** 1628

[60] Ahmadi T S, Wang Z L, Green T C, Henglein A and El-Sayed M A 1996 *Science* **262** 1924

[61] Haruta M 2003 *J. Nanopart. Res.* **5** 3

[61] Choudary B M, Mulukutla R S and Klabunde K J 2003 *J. Am.Chem. Soc.* **125** 2020

[63] Narayanan R and El-Sayed M A 2004 *Nano Lett.* **4** 1343

[64] Telkar M M, Rode C V, Chaudhari R V, Joshi S S and Nalawade A M 2004 *Appl. Catal.* A **263** 11

[65] Somorjai G A and Yang M 2003 *Top. Catal.* **24** 61

[66] Weiss W and Ranke W 2002 *Prog. Surf. Sci.* **60** 1

[67] Vesecky S M, Rainer D R and Goodman D W 1996 *J. Vac. Sci.Technol.* A **14** 1456

[68] Ertl G and Freund H J 1999 *Phys. Today* **52** 32

[69] Zhou K B, Wang X, Sun X M, Peng Q and Li Y D 2005 *J. Catal.* **229** 206

[70] Zhou K B, Xu R, Sun X M, Chen H D, Tian Q, Shen D X and Li Y D 2005 *Catal. Lett.* **101** 169

[71] Jernigan G G and Somorjai G A 1994 *J. Catal.* **146** 566

[72] Sadykov V A and Tikhov S F 1996 *J. Catal.* **165** 269

[73] Nagase K, Zheng Y, Kodama Y and Kakuta J 1999 *J. Catal.***186** 123

[74] Huang T J and Tsai D H 2003 *Catal. Lett.* **86** 163

[75] Jiang X C, Herricks T and Xia Y N 2002 *Nano Lett.* **2** 1333

[76] Lu C H, Qi L M, Yang J H, Zhang D Y, Wu N Z and Ma J M 2004 *J. Phys. Chem.* B **108** 16825

[77] Wang Z L, Kong X Y,Wen X G and Yang S H 2003 *J. Phys.Chem.* B **106** 8265

[78] Liu B and Zeng H C 2004 *J. Am. Chem. Soc.* **126** 8124

[79] Chang Y and Zeng H C 2004 *Cryst. Growth Des.* **4** 396

[80]. Lee S and Choi S. U. S (1996). Applications of metallic nanoparticle suspensions in advanced cooling systems, in Recent Advances in Solids/Structures and Applications of Metallic Materials. American Society of Mechnaical Engineers, Volume 40. pp. 226-234.

[81]. Chien H.T, Tsai C.I, Chen P. H, and Chen P.Y (2003). Improvement on thermal performance of a disk-shaped miniature heat pipe with nanofluid. Proc. International Conference on Electronics Packaging Technology, IEEE, Piscatway, NJ. pp. 389-391.

[82]. Tzeng S C, Lin C W, and Huang K D (2005). Heat transfer enhancement of nanofluids in rotary blade coupling of four wheel drive vehicles. Acta Mech, Volume 169. pp. 11-23.

[83]. Xuan Y and Li Q (2000). Heat transfer enhancement of nanofluids. Int. J. Heat fluid flow, Volume 21. Issue 1. pp. 58-64.

[84]. Yu W, Choi S. U. S, and Drobnik J (2006). Temperature and concentration dependence of effective thermal conductivities of alumina oil based nanofluids. ECI Conference on Nanofluids: Fundamental and Application Copper Mountain, Colorado, Sept 16-20.

[85]. You S. M, Kim J. H, and Kim K. M (2003). Effect of nanoparticles on critical heat flux of water in pool boiling of heat transfer. Appl. Phys. Lett, Volume 83. pp. 3364-3366.

[86]. Kim S. J, Bang I. C, Buongiorono J, and Hu L.W (2006). Effects of nanoparticles deposition on surface wettability influencing boiling heat transfer in nanofluids. Appl. Phys Lett, Volume 89. Issue 15. pp. 3106.

[87]. Granqvist, C.G., and R.A.Buhrman (1976). Ultrafine metal particles, J. Appl. Phys., 47:2200.

[88]. Hornyak G., Dutta J., Tibbals H., Rao A. (2008). Introduction of nanoscience. Taylor & Francis. pp. 108-115.

ANNEXTURE-I

Ethylene glycol with CuO at 0.005%

At Temperature 25^{o}C

RPM	VISCOSITY	SHEAR STRESS (d/cm^2)	SHEAR RATE
10	16	6.06	38
15	16	9.1	57
20	16	12.1	76
25	16	15.2	95
30	16	18.2	114
35	16	21.2	133

At Temperature 30^{o}C

RPM	VISCOSITY	SHEAR STRESS (d/cm^2)	SHEAR RATE
10	13	4.95	38
15	13	7.43	57
20	13	9.89	76
25	13	12.4	95
30	13	14.8	114

35	13	17.3	133
40	13	19.8	152
45	13	22.2	171

At Temperature 35^{o}C

RPM	VISCOSITY	SHEAR STRESS (d/cm^2)	SHEAR RATE
10	10.7	4.6	38
15	10.7	6.09	57
20	10.7	8.14	76
25	10.7	10.1	95
30	10.7	12.2	114
35	10.7	14.2	133
40	10.7	16.2	152
45	10.7	18.3	171
50	10.7	20.3	190

At Temperature 40^{o}C

RPM	VISCOSITY	SHEAR STRESS (d/cm^2)	SHEAR RATE
10	8.88	3.37	38
15	8.88	5.06	57
20	8.88	6.77	76
25	8.88	8.46	95
30	8.88	10.2	114
35	8.88	11.8	133
40	8.88	13.5	152
45	8.88	15.2	171
50	8.88	16.9	190

At Temperature 45^{o}C

RPM	VISCOSITY	SHEAR STRESS (d/cm^2)	SHEAR RATE
10	7.44	2.83	38
15	7.44	4.24	57
20	7.44	5.68	76
25	7.44	7.09	95
30	7.44	8.53	114
35	7.44	9.92	133
40	7.44	11.3	152
45	7.44	12.7	171
50	7.44	14.2	190

At Temperature 50^{o}C

RPM	VISCOSITY	SHEAR STRESS (d/cm^2)	SHEAR RATE

10	6.3	2.83	38
15	6.28	3.6	57
20	6.3	4.81	76
25	6.31	6	95
30	6.3	7.18	114
35	6.31	8.39	133
40	6.33	9.6	152
45	6.32	10.8	171
50	6.32	12	190

Ethylene glycol with CuO at 0.01%

At Temperature 25^{o}C

RPM	VISCOSITY	SHEAR STRESS (d/cm^2)	SHEAR RATE
10	16.4	6.27	38
15	16.3	9.28	57
20	15.8	12	76
25	15.7	14.9	95
30	15.7	17.9	114
35	15.7	20.9	133

At Temperature 30^{o}C

RPM	VISCOSITY	SHEAR STRESS (d/cm^2)	SHEAR RATE
10	12.9	4.9	38
15	12.9	7.32	57
20	12.8	9.76	76
25	12.8	12.1	95
30	12.8	14.6	114
35	12.8	17	133
40	12.8	19.4	152
45	12.8	21.8	171

At Temperature 35^{o}C

RPM	VISCOSITY	SHEAR STRESS (d/cm^2)	SHEAR RATE
10	10.5	3.97	38
15	10.5	6	57
20	10.5	7.96	76
25	10.5	9.94	95
30	10.5	12	114
35	10.5	14	133

40	10.5	16	152
45	10.5	18	171
50	10.5	20	190

At Temperature 40^{o}C

RPM	VISCOSITY	SHEAR STRESS (d/cm^2)	SHEAR RATE
10	8.7	3.3	38
15	8.68	4.95	57
20	8.67	6.51	76
25	8.69	8.25	95
30	8.72	9.94	114
35	8.72	11.6	133
40	8.74	13.3	152
45	8.7	14.9	171
50	8.7	16.5	190

At Temperature 45^{o}C

RPM	VISCOSITY	SHEAR STRESS (d/cm^2)	SHEAR RATE
10	7.32	2.76	38
15	7.28	4.13	57
20	7.26	5.52	76
25	7.25	6.88	95
30	7.28	8.3	114
35	7.28	9.69	133
40	7.3	11.1	152
45	7.29	12.5	171
50	7.29	13.9	190

At Temperature 50^{o}C

RPM	VISCOSITY	SHEAR STRESS (d/cm^2)	SHEAR RATE
10	6.12	2.33	38
15	6.16	3.51	57
20	6.18	4.7	76
25	6.19	5.86	95
30	6.18	7.09	114
35	6.17	8.23	133
40	6.19	9.39	152
45	6.16	10.5	171
50	6.19	11.8	190

Ethylene glycol with CuO at 0.05%

At Temperature 25^{o}C

RPM	VISCOSITY	SHEAR STRESS (d/cm^2)	SHEAR RATE
10	16.3	6.15	38
15	16.3	9.23	57
20	16.3	12.4	76
25	16.3	15.5	95
30	16.3	18.6	114
35	16.3	21.7	133

At Temperature 30^{o}C

RPM	VISCOSITY	SHEAR STRESS (d/cm^2)	SHEAR RATE
10	13.3	5.04	38
15	13.3	7.57	57
20	13.3	10.1	76
25	13.3	12.6	95
30	13.3	15.1	114
35	13.3	17.6	133
40	13.3	20.2	152
45	13.3	22.7	171

At Temperature 35^{o}C

RPM	VISCOSITY	SHEAR STRESS (d/cm^2)	SHEAR RATE
10	10.9	4.14	38
15	10.9	6.22	57
20	10.9	8.27	76
25	10.9	10.3	95
30	10.9	12.4	114
35	10.9	14.5	133
40	10.9	16.6	152
45	10.9	18.7	171
50	10.9	20.7	190

At Temperature 40^{o}C

RPM	VISCOSITY	SHEAR STRESS (d/cm^2)	SHEAR RATE
10	9.06	3.44	38
15	8.96	5.15	57

20	8.94	6.79	76
25	8.97	8.5	95
30	9	10.3	114
35	9.02	12	133
40	9.04	13.7	152
45	9.01	15.4	171
50	8.97	17	190

At Temperature 45^{o}C

RPM	VISCOSITY	SHEAR STRESS (d/cm^2)	SHEAR RATE
10	7.62	2.92	38
15	7.64	4.33	57
20	7.62	5.79	76
25	7.61	7.23	95
30	7.62	8.66	114
35	7.61	10.1	133
40	7.59	11.6	152
45	7.57	13	171
50	7.57	14.4	190

At Temperature 50^{o}C

RPM	VISCOSITY	SHEAR STRESS (d/cm^2)	SHEAR RATE
10	6.42	2.46	38
15	6.48	3.69	57
20	6.42	4.88	76
25	6.41	6.11	95
30	6.46	7.36	114
35	6.46	8.57	133
40	6.45	9.8	152
45	6.45	11	171
50	6.44	12.8	190

Ethylene glycol with CuO at 0.1%

At Temperature 25^{o}C

RPM	VISCOSITY	SHEAR STRESS	SHEAR RATE

		(d/cm^2)	
10	15.8	6.02	38
15	15.8	9	57
20	15.8	12	76
25	15.8	15	95
30	15.9	18	114
35	15.9	21.1	133

At Temperature 30^{o}C

RPM	VISCOSITY	SHEAR STRESS (d/cm^2)	SHEAR RATE
10	12.8	4.83	38
15	12.8	7.29	57
20	12.8	9.71	76
25	12.8	12.2	95
30	12.9	14.7	114
35	12.9	17.1	133
40	12.9	19.6	152
45	12.9	21.9	171

At Temperature 35^{o}C

RPM	VISCOSITY	SHEAR STRESS (d/cm^2)	SHEAR RATE
10	10.5	4.01	38
15	10.5	5.97	57
20	10.5	7.98	76
25	10.5	9.98	95
30	10.5	12	114
35	10.5	14	133
40	10.5	16	152
45	10.5	18	171
50	10.5	20	190

At Temperature 40^{o}C

RPM	VISCOSITY	SHEAR STRESS (d/cm^2)	SHEAR RATE
10	8.73	3.31	38
15	8.72	4.97	57
20	8.7	6.63	76
25	8.72	8.27	95
30	8.72	9.92	114
35	8.71	11.6	133
40	8.7	13.2	152
45	8.7	14.9	171
50	8.7	16.5	190

At Temperature 45^{o}C

RPM	VISCOSITY	SHEAR STRESS (d/cm^2)	SHEAR RATE
10	7.32	2.78	38
15	7.32	4.17	57
20	7.32	5.56	76
25	7.32	6.93	95
30	7.32	8.34	114
35	7.32	9.73	133
40	7.32	11.1	152
45	7.32	12.5	171
50	7.32	13.9	190

At Temperature 50^{o}C

RPM	VISCOSITY	SHEAR STRESS (d/cm^2)	SHEAR RATE
10	6.24	2.37	38
15	6.24	3.58	57
20	6.24	4.76	76
25	6.24	5.9	95
30	6.24	7.13	114
35	6.24	8.32	133
40	6.24	9.51	152
45	6.24	10.7	171
50	6.24	11.9	190

ANNEXTURE-II

Ethylene glycol with water (60:40)

At Temperature 25^{o}C

RPM	VISCOSITY	SHEAR STRESS (d/cm^2)	SHEAR RATE
10	4.14	1.55	38
15	4.12	2.33	57
20	4.08	3.1	76
25	4.06	3.88	95
30	4.06	4.63	114
35	4.04	5.38	133
40	4.03	6.15	152
45	4.04	6.93	171
50	4.03	7.66	190

At Temperature 30^{o}C

RPM	VISCOSITY	SHEAR STRESS (d/cm^2)	SHEAR RATE
10	3.48	1.34	38
15	3.48	1.98	57
20	3.48	2.62	76
25	3.48	3.31	95
30	3.48	3.97	114
35	3.46	4.6	133
40	3.45	5.24	152
45	3.45	5.9	171
50	3.44	6.56	190

At Temperature 35^{o}C

RPM	VISCOSITY	SHEAR STRESS (d/cm^2)	SHEAR RATE
10	3	1.14	38
15	3	1.71	57
20	3	2.3	76
25	3	2.85	95
30	3	3.44	114
35	3	4.01	133
40	3	4.56	152

45	3	5.13	171
50	3	5.7	190

At Temperature 40^{o}C

RPM	VISCOSITY	SHEAR STRESS (d/cm^2)	SHEAR RATE
10	2.64	1.03	38
15	2.64	1.5	57
20	2.64	2.01	76
25	2.64	2.51	95
30	2.64	3.01	114
35	2.64	3.51	133
40	2.64	4.01	152
45	2.64	4.49	171
50	2.64	4.99	190

At Temperature 45^{o}C

RPM	VISCOSITY	SHEAR STRESS (d/cm^2)	SHEAR RATE
10	2.28	0.87	38
15	2.28	1.32	57
20	2.28	1.76	76
25	2.28	2.21	95
30	2.28	2.62	114
35	2.28	3.05	133
40	2.28	3.51	152
45	2.28	3.94	171
50	2.28	4.4	190

At Temperature 50^{o}C

RPM	VISCOSITY	SHEAR STRESS (d/cm^2)	SHEAR RATE
10	2.04	0.8	38
15	2.04	1.14	57
20	2.04	1.55	76
25	2.04	1.96	95
30	2.04	2.33	114

35	2.04	2.71	133
40	2.04	3.12	152
45	2.04	3.49	171
50	2.04	3.88	190

Ethylene glycol with water (60:40 by weight) for volumetric concentration 0.005%

At Temperature 25^{o}C

RPM	VISCOSITY	SHEAR STRESS (d/cm^2)	SHEAR RATE
10	4.5	1.71	38
15	4.52	2.58	57
20	4.5	3.42	76
25	4.49	4.26	95
30	4.48	5.13	114
35	4.49	5.97	133
40	4.5	6.84	152
45	4.51	7.7	171
50	4.5	8.53	190

At Temperature 30^{o}C

RPM	VISCOSITY	SHEAR STRESS (d/cm^2)	SHEAR RATE
10	3.84	1.46	38
15	3.84	2.19	57
20	3.84	2.92	76
25	3.84	3.65	95
30	3.84	4.35	114
35	3.84	5.06	133
40	3.82	5.81	152
45	3.83	6.54	171
50	3.82	7.27	190

At Temperature 35^{o}C

RPM	VISCOSITY	SHEAR STRESS (d/cm^2)	SHEAR RATE
10	3.3	1.25	38
15	3.28	1.89	57
20	3.27	2.48	76

25	3.29	3.12	95
30	3.29	3.74	114
35	3.29	4.38	133
40	3.28	4.99	152
45	3.29	5.63	171
50	3.3	6.27	190

At Temperature 40^{o}C

RPM	VISCOSITY	SHEAR STRESS (d/cm^2)	SHEAR RATE
10	2.88	1.09	38
15	2.88	1.62	57
20	2.85	2.17	76
25	2.83	2.69	95
30	2.84	3.24	114
35	2.85	3.78	133
40	2.85	4.33	152
45	2.85	4.88	171
50	2.86	5.43	190

At Temperature 45^{o}C

RPM	VISCOSITY	SHEAR STRESS (d/cm^2)	SHEAR RATE
10	2.46	0.91	38
15	2.44	1.39	57
20	2.46	1.89	76
25	2.47	2.33	95
30	2.48	2.8	114
35	2.47	3.28	133
40	2.49	3.78	152
45	2.48	4.24	171
50	2.48	4.74	190

At Temperature 50^{o}C

RPM	VISCOSITY	SHEAR STRESS (d/cm^2)	SHEAR RATE
10	2.16	0.82	38
15	2.16	1.23	57
20	2.16	1.64	76
25	2.18	2.07	95
30	2.2	2.51	114
35	2.19	2.92	133
40	2.2	3.35	152
45	2.2	3.74	171
50	2.21	4.19	190

Ethylene glycol with water (60:40 by weight) for volumetric concentration 0.05%

At Temperature 25^{o}C

RPM	VISCOSITY	SHEAR STRESS (d/cm^2)	SHEAR RATE
10	4.56	1.73	38
15	4.56	2.6	57
20	4.53	3.44	76
25	4.49	4.29	95
30	4.5	5.13	114
35	4.51	5.97	133
40	4.5	6.84	152
45	4.5	7.73	171
50	4.5	8.55	190

At Temperature 30^{o}C

RPM	VISCOSITY	SHEAR STRESS (d/cm^2)	SHEAR RATE
10	3.84	1.46	38
15	3.84	2.19	57
20	3.84	2.94	76
25	3.84	3.67	95
30	3.84	4.35	114
35	3.84	5.08	133
40	3.84	5.84	152
45	3.83	6.54	171
50	3.83	7.27	190

At Temperature 35^{o}C

RPM	VISCOSITY	SHEAR STRESS (d/cm^2)	SHEAR RATE
10	3.3	1.25	38
15	3.28	1.89	57
20	3.27	2.51	76
25	3.29	3.12	95
30	3.3	3.74	114
35	3.29	4.35	133
40	3.28	4.99	152

45	3.29	5.63	171
50	3.29	6.25	190

At Temperature 40^{o}C

RPM	VISCOSITY	SHEAR STRESS (d/cm^2)	SHEAR RATE
10	2.94	1.09	38
15	2.88	1.64	57
20	2.88	2.19	76
25	2.88	2.71	95
30	2.86	3.28	114
35	2.85	3.78	133
40	2.85	4.35	152
45	2.85	4.88	171
50	2.84	5.43	190

At Temperature 45^{o}C

RPM	VISCOSITY	SHEAR STRESS (d/cm^2)	SHEAR RATE
10	2.53	0.96	38
15	2.53	1.44	57
20	2.53	1.89	76
25	2.53	2.39	95
30	2.53	2.83	114
35	2.5	3.31	133
40	2.5	3.78	152
45	2.5	4.24	171
50	2.5	4.74	190

At Temperature 50^{o}C

RPM	VISCOSITY	SHEAR STRESS (d/cm^2)	SHEAR RATE
10	2.22	0.84	38
15	2.2	1.25	57
20	2.22	1.69	76
25	2.21	2.12	95
30	2.2	2.53	114
35	2.19	2.94	133
40	2.19	3.35	152
45	2.2	3.78	171
50	2.2	4.19	190